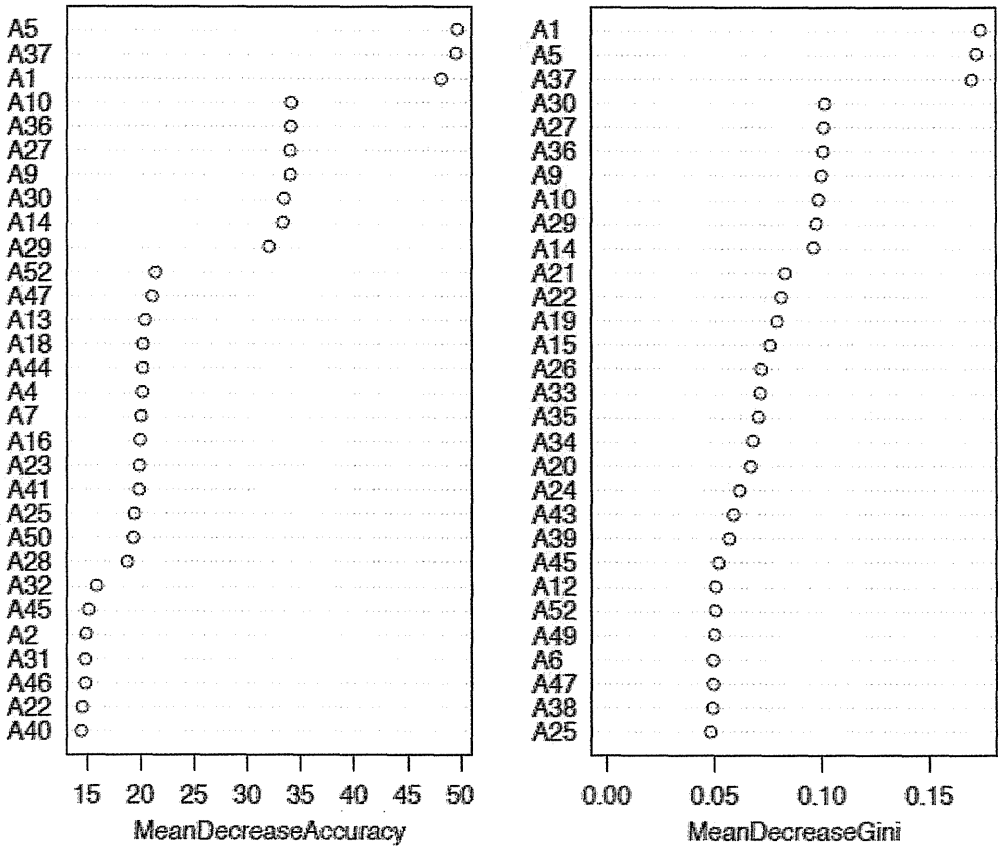

Additional File 2. RF Dotchart of variable importance for vehicle control *vs.* MGT-treated group.

Additional File 3. Information of the authentic DNA adducts.

Adduct	Precurser (M + H)	Product (Deoxyribose Loss)	Ref.	Na 22.9898	K 39.0983	NH_3 18.0379
5-MedC	242.1140	126.0666	-	264.0960	280.2045	259.1441
dU	229.0824	113.0350	[36]	251.0644	267.1729	246.1125
dI	253.0936	137.0462	[36]	275.0756	291.1841	270.1237
dX	269.0886	153.0412	[36]	291.0706	307.1791	286.1187
dO	269.0886	153.0412	[36]	291.0706	307.1791	286.1187
8-Oxo-dG	284.0994	168.0520	[37]	306.0814	322.1899	301.1295
Sp	300.0944	184.0470	[38]	322.0764	338.1849	317.1245
Gh	274.1151	158.0677	[38]	296.0971	312.2056	291.1452
Iz	229.0937	113.0463	[38]	251.0757	267.1842	246.1238
Oz	247.1042	131.0568	[39]	269.0862	285.1947	264.1343
FapyG	286.1151	170.0677	[39]	308.0971	324.2056	303.1452
Oxa	249.0723	133.0249	[38]	271.0543	287.1628	266.1024
Cyclo-dG	266.0889	150.0415	[40]	288.0709	304.1794	283.1190
Cyanuric acid	246.0726	130.0252	[38]	268.0546	284.1631	263.1027
CAC	288.0944	172.0470	[41]	310.0764	326.1849	305.1245
HICA	277.0672	161.0198	[41]	299.0492	315.1577	294.0973
8-OH-dA	268.1046	152.0572	[39]	290.0866	306.1951	285.1347

Additional File 3. *Cont.*

Adduct	Precurser (M + H)	Product (Deoxyribose Loss)	Ref.	Na 22.9898	K 39.0983	NH_3 18.0379
2-OH-dA	268.1046	152.0572	[42]	290.0866	306.1951	285.1347
FapydA	270.1202	154.0728	[39]	292.1022	308.2107	287.1503
Cyclo-dA	250.0940	134.0466	[39]	272.0760	288.1845	267.1241
5-OHdC	244.0933	128.0459	[39]	266.0753	282.1838	261.1234
5-HmdU	259.0930	143.0456	[39]	281.0750	297.1835	276.1231
FodU	257.0773	141.0299	[39]	279.0593	295.1678	274.1074
Tg	277.1036	161.0562	[39]	299.0856	315.1941	294.1337
d(G[8–5]C)	555.1353	439.0879	[43]	515.1615	531.2700	510.2096
d(G[8–3]T)	508.1792	392.1318	[44]	530.1612	546.2697	525.2093
d(G[8–5m]T)	508.1792	392.1318	[45]	530.1612	546.2697	525.2093
εdA	276.1096	160.0622	[39]	298.0916	314.2001	293.1397
εdC	252.0984	136.0510	[39]	274.0804	290.1889	269.1285
ε5mdC	266.1100	150.0626	[46]	288.0920	304.2005	283.1401
εdG	292.1046	176.0572	[39]	314.0866	330.1951	309.1347
M1dG	304.1046	188.0572	[39]	326.0866	342.1951	321.1347
5,6-dihydro-M1dG	306.1202	190.0728	[47]	328.1022	344.2107	323.1503
PdG	308.1359	192.0885	[39]	330.1179	346.2264	325.1660
6-oxo-M1dG	320.0995	204.0521	[48]	342.0815	358.1900	337.1296
MDA-dA	306.1202	190.0728	[49]	328.1022	344.2107	323.1503
MDA-dC	282.1090	166.0616	[49]	304.0910	320.1995	299.1391
8-OH-PdG	324.1307	208.0833	[50]	346.1127	362.2212	341.1608
6-OH-PdG	324.1307	208.0833	[50]	346.1127	362.2212	341.1608
propano-dA	308.1359	192.0885	[51]	330.1179	346.2264	325.1660
propano-dC	286.1403	170.0929	[51] *	308.1223	324.2308	303.1704
propano-5MedC	300.1560	184.1086	[51] *	322.1380	338.2465	317.1861
FDP-dG	362.1465	246.0991	[52] *	384.1285	400.2370	379.1766
α-Me-γ-OH-PdG (R- or S-α-Me-γ-OH-CRA-dG)	338.1464	222.0990	[50]	360.1284	376.2369	355.1765
Croton-dA	322.1516	206.1042	[50] *	344.1336	360.2421	339.1817
Croton-dC	300.1560	184.1086	[50] *	322.1380	338.2465	317.1861
Croton-5MedC	314.1717	198.1243	[50] *	336.1537	352.2622	331.2018
ICL-RD	589.2483	473.2009	[53]	611.2303	627.3388	606.2784
ICL-R	587.2326	471.1852	[53]	609.2146	625.3231	604.2627
ICL-S	587.2326	471.1852	[53]	609.2146	625.3231	604.2627
Hexanoyl-dG	366.1777	250.1303	[54] *	388.1597	404.2682	383.2078
Hexenal-dG	366.1777	250.1303	[55]	388.1597	404.2682	383.2078
HNE-dG	424.2196	308.1722	[56]	446.2016	462.3101	441.2497
HNE-dA	408.2248	292.1774	[56] *	430.2068	446.3153	425.2549
HNE-dC	386.2292	270.1818	[56] *	408.2112	424.3197	403.2593
HNE-5MedC	400.2449	284.1975	[56] *	422.2269	438.3354	417.2750
HεdG	404.1933	288.1459	[57]	426.1753	442.2838	421.2234

Additional File 3. *Cont.*

Adduct	Precurser (M + H)	Product (Deoxyribose Loss)	Ref.	Na 22.9898	K 39.0983	NH_3 18.0379
HεdA	388.1984	272.1510	[57]	410.1804	426.2889	405.2285
HεdC	364.1872	248.1398	[57]	386.1692	402.2777	381.2173
HεMedC	378.2029	262.1555	[57] *	400.1849	416.2934	395.2330
BεdG	362.1464	246.0990	[58]	384.1284	400.2369	379.1765
BεdA	346.1515	230.1041	[58] *	368.1335	384.2420	363.1816
BεdC	322.1402	206.0928	[58]	344.1222	360.2307	339.1703
BεMedC	336.1559	220.1085	[58]	358.1379	374.2464	353.1860
CHPdG	460.2196	344.1722	[59] *	482.2016	498.3101	477.2497
CHPdA	444.2247	328.1773	[59] *	466.2067	482.3152	461.2548
CHPdC	420.2134	304.1660	[59] *	442.1954	458.3039	437.2435
CPPdG	404.1570	288.1096	[59] *	426.1390	442.2475	421.1871
CPPdA	388.1621	272.1147	[59] *	410.1441	426.2526	405.1922
CPPdC	364.1508	248.1034	[59] *	386.1328	402.2413	381.1809
CEPdG	390.1413	274.0939	[59] *	412.1233	428.2318	407.1714
CEPdA	374.1464	258.0990	[59] *	396.1284	412.2369	391.1765
CEPdC	350.1352	234.0878	[59] *	372.1172	388.2257	367.1653
N^6-HmdA	282.1202	166.0728	[60]	304.1022	320.2107	299.1503
N^6-MedA	266.1253	150.0779	[61]	288.1073	304.2158	283.1554
N^2-Ethylidene-dG	294.1202	178.0728	[62]	316.1022	332.2107	311.1503
N^2-ethyl-dG	296.1359	180.0885	[62]	318.1179	334.2264	313.1660
1-medA	268.1409	152.0935	[38]	290.1229	306.2314	285.1710
3-medC	243.1213	127.0739	[38]	265.1033	281.2118	260.1514
N^2-CMdG	326.1100	210.0626	[63]	348.0920	364.2005	343.1401
Glyoxal-dA	310.1152	194.0678	[63]	332.0972	348.2057	327.1453
Glyoxal-dC	288.1196	172.0722	[63]	310.1016	326.2101	305.1497
Glyoxal-5MedC	302.1353	186.0879	[63] *	324.1173	340.2258	319.1654
N^2-CEdG	340.1257	224.0783	[64]	362.1077	378.2162	357.1558
8-Cl-dG	302.0656	186.01824	[65]	324.0476	340.1561	319.0957
8-Cl-dA	286.0707	170.02334	[65]	308.0527	324.1612	303.1008
5-Cl-dC	262.0594	146.01204	[65]	284.0414	300.1499	279.0895
8-Br-dG	346.0151	229.96774	[66]	367.9971	384.1056	363.0452
8-Br-dA	330.0202	213.97284	[66] *	352.0022	368.1107	347.0503
5-Br-dC	306.0089	189.96154	[67]	327.9909	344.0994	323.039

Na: sodium added form; K: potassium added form; NH_3: ammonium added form; *: Expected *m/z* calculated by Symyx Draw 4.0 software (Accelrys Inc., San Diego, CA, USA).

Conflicts of Interest

The authors declare no conflict of interest.

References

1. Cabreraa, L.; Gutierreza, S.; Menendezb, N.; Moralesc, M.P.; Herrasti, P. Magnetite nanoparticles: Electrochemical synthesis and characterization. *Electrochim. Acta* **2008**, *53*, 3436–3441.

2. Jin, R.; Lin, B.; Li, D.; Ai, H. Superparamagnetic iron oxide nanoparticles for MR imaging and therapy: Design considerations and clinical applications. *Curr. Opin. Pharmacol.* **2014**, *18C*, 18–27.
3. Felton, C.; Karmakar, A.; Gartia, Y.; Ramidi, P.; Biris, A.S.; Ghosh, A. Magnetic nanoparticles as contrast agents in biomedical imaging: Recent advances in iron- and manganese-based magnetic nanoparticles. *Drug Metab. Rev.* **2014**, *46*, 142–154.
4. Guichard, Y.; Schmit, J.; Darne, C.; Gaté, L.; Goutet, M.; Rousset, D.; Rastoix, O.; Wrobel, R.; Witschger, O.; Martin, A.; *et al.* Cytotoxicity and genotoxicity of nanosized and microsized titanium dioxide and iron oxide particles in Syrian hamster embryo cells. *Ann. Occup. Hyg.* **2012**, *56*, 631–644.
5. Aranda, A.; Sequedo, L.; Tolosa, L.; Quintas, G.; Burello, E.; Castell, J.V.; Gombau, L. Dichloro-dihydro-fluorescein diacetate (DCFH-DA) assay. A quantitative method for oxidative stress assessment of nanoparticle-treated cells. *Toxicol. Vitro* **2013**, *27*, 954–963.
6. Singh, N.; Jenkins, G.J.; Asadi, R.; Doak, S.H. Potential toxicity of superparamagnetic iron oxide nanoparticles (SPION). *Nano Rev.* **2010**, *1*, 5358–5373.
7. Ramesh, V.; Ravichandran, P.; Copeland, C.L.; Gopikrishnan, R.; Biradar, S.; Goornavar, V.; Ramesh, G.T.; Hall, J.C. Magnetite induces oxidative stress and apoptosis in lung epithelial cells. *Mol. Cell Biochem.* **2012**, *363*, 225–234.
8. Könczöl, M.; Ebeling, S.; Goldenberg, E.; Treude, F.; Gminski, R.; Gieré, R.; Grobéty, B.; Rothen-Rutishauser, B.; Merfort, I.; Mersch-Sundermann, V. Cytotoxicity and genotoxicity of size-fractionated iron oxide (magnetite) in A549 human lung epithelial cells: Role of ROS, JNK, and NF-κB. *Chem. Res. Toxicol.* **2011**, *24*, 1460–1475.
9. Karlsson, H.L.; Gustafsson, J.; Cronholm, P.; Möller, L. Size-dependent toxicity of metal oxide particles—A comparison between nano- and micrometer size. *Toxicol. Lett.* **2009**, *188*, 112–118.
10. Ma, P.; Luo, Q.; Chen, J.; Gan, Y.; Du, J.; Ding, S.; Xi, Z.; Yang, X. Intraperitoneal injection of magnetic Fe_3O_4-nanoparticle induces hepatic and renal tissue injury via oxidative stress in mice. *Int. J. Nanomed.* **2012**, *7*, 4809–4818.
11. Weissleder, R.; Stark, D.D.; Engelstad, B.L.; Bacon, B.R.; Compton, C.C.; White, D.L.; Jacobs, P.; Lewis, J. Superparamagnetic iron oxide: Pharmacokinetics and toxicity. *Am. J. Roentgenol.* **1989**, *152*, 167–173.
12. Singh, N.; Jenkins, G.J.; Nelson, B.C.; Marquis, B.J.; Maffeis, T.G.; Brown, A.P.; Williams, P.M.; Wright, C.J.; Doak, S.H. The role of iron redox state in the genotoxicity of ultrafine superparamagnetic iron oxide nanoparticles. *Biomaterials* **2012**, *33*, 163–170.
13. Szalay, B.; Tátrai, E.; Nyírő, G.; Vezér, T.; Dura, G. Potential toxic effects of iron oxide nanoparticles in *in vivo* and *in vitro* experiments. *J. Appl. Toxicol.* **2012**, *32*, 446–453.
14. Watanabe, M.; Yoneda, M.; Morohashi, A.; Okamoto, D.; Sato, A.; Kurioka, D.; Hirokawa, H.; Shiraishi, T.; Kawai, K.; Kasai, K.; *et al.* Effects of Fe_3O_4-based magnetic nanoparticles on A549 cells. *Int. J. Mol. Sci.* **2013**, *14*, 15546–15560.
15. Kawanishi, M.; Ogo, S.; Ikemoto, M.; Totsuka, Y.; Ishino, K.; Wakabayahsi, K.; Yagi, T. Genotoxicity and reactive oxygen species production induced by magnetite nanoparticles in mammalian cells. *J. Toxicol. Sci.* **2013**, *38*, 503–511.

16. Totsuka, Y.; Ishino, K.; Kato, T.; Goto, S.; Tada, Y.; Nakae, D.; Watanabe, M.; Wakabayashi, K. Magnetite nanoparticles induce genotoxicity in the lungs of mice via inflammatory response. *Nanomaterials* **2014**, *4*, 175–188.
17. Kew, M.C. Aflatoxins as a cause of hepatocellular carcinoma. *J. Gastrointest. Liver Dis.* **2013**, *22*, 305–310.
18. Hollstein, M.; Moriya, M.; Grollman, A.P.; Olivier, M. Analysis of TP53 mutation spectra reveals the fingerprint of the potent environmental carcinogen, aristolochic acid. *Mutat. Res.* **2013**, *753*, 41–49.
19. Hecht, S.S. Lung carcinogenesis by tobacco smoke. *Int. J. Cancer* **2012**, *131*, 2724–2732.
20. Khalili, H.; Zhang, F.J.; Harvey, R.G.; Dipple, A. Mutagenicity of benzo[*a*]pyrene-deoxyadenosine adducts in a sequence context derived from the *p53* gene. *Mutat. Res.* **2000**, *465*, 39–44.
21. Scholdberg, T.A.; Nechev, L.V.; Merritt, W.K.; Harris, T.M.; Harris, C.M.; Lloyd, R.S.; Stone, M.P. Mispairing of a site specific major groove (2S,3S)-N^6-(2,3,4-trihydroxybutyl)-2'-deoxyadenosyl DNA Adduct of butadiene diol epoxide with deoxyguanosine: Formation of a dA(anti)·dG(anti) pairing interaction. *Chem. Res. Toxicol.* **2005**, *18*, 145–153.
22. Pollack, M.; Yang, I.Y.; Kim, H.Y.; Blair, I.A.; Moriya, M. Translesion DNA Synthesis across the heptanone-etheno-2'-deoxycytidine adduct in cells. *Chem. Res. Toxicol.* **2006**, *19*, 1074–1079.
23. Yang, I.Y.; Hashimoto, K.; de Wind, N.; Blair, I.A.; Moriya, M. Two distinct translesion synthesis pathways across a lipid peroxidation-derived DNA adduct in mammalian cells. *J. Biol. Chem.* **2009**, *284*, 191–198.
24. Kanaly, R.A.; Hanaoka, T.; Sugimura, H.; Toda, H.; Matsui, S.; Matsuda, T. Development of the adductome approach to detect DNA damage in humans. *Antioxid. Redox Signal.* **2006**, *8*, 993–1001.
25. Matsuda, T.; Tao, H.; Goto, M.; Yamada, H.; Suzuki, M.; Wu, Y.; Xiao, N.; He, Q.; Guo, W.; Cai, Z.; *et al.* Lipid peroxidation-induced DNA adducts in human gastric mucosa. *Carcinogenesis* **2013**, *34*, 121–127.
26. Park, E.J.; Kim, H.; Kim, Y.; Yi, J.; Choi, K.; Park, K. Inflammatory responses may be induced by a single intratracheal instillation of iron nanoparticles in mice. *Toxicology* **2010**, *275*, 65–71.
27. Hsiao, J.K.; Weng, T.I.; Tai, M.F.; Chen, Y.F.; Wang, Y.H.; Yang, C.Y.; Wang, J.L.; Liu, H.M. Cellular behavior change of macrophage after exposure to nanoparticles. *J. Nanosci. Nanotechnol.* **2009**, *9*, 1388–1393.
28. Xia, T.; Kovochich, M.; Liong, M.; Zink, J.I.; Nel, A.E. Cationic polystyrene nanosphere toxicity depends on cell-specific endocytic and mitochondrial injury pathways. *ACS Nano* **2008**, *2*, 85–96.
29. He, X.; Young, S.H.; Schwegler-Berry, D.; Chisholm, W.P.; Fernback, J.E.; Ma, Q. Multiwalled carbon nanotubes induce a fibrogenic response by stimulating reactive oxygen species production, activating NF-κB signaling, and promoting fibroblast-to-myofibroblast transformation. *Chem. Res. Toxicol.* **2011**, *24*, 2237–2248.
30. Kasper, J.L.; Hermanns, M.I.; Bantz, C.; Maskos, M.; Stauber, R.; Pohl, C.; Unger, R.E.; Kirkpatrick, J.C. Inflammatory and cytotoxic responses of an alveolar-capillary coculture model to silica nanoparticles: Comparison with conventional monocultures. *Part. Fibre Toxicol.* **2011**, *8*, 6, doi:10.1186/1743-8977-8-6.

31. Dostert, C.; Pétrilli, V.; van Bruggen, R.; Steele, C.; Mossman, B.T.; Tschopp, J. Innate immune activation through Nalp3 inflammasome sensing of asbestos and silica. *Science* **2008**, *320*, 674–677.
32. Cassel, S.L.; Eisenbarth, S.C.; Iyer, S.S.; Sadler, J.J.; Colegio, O.R.; Tephly, L.A.; Carter, A.B.; Rothman, P.B.; Flavell, R.A.; Sutterwala, F.S. The Nalp3 inflammasome is essential for the development of silicosis. *Proc. Natl. Acad. Sci. USA* **2008**, *105*, 9035–9040.
33. Matsuda, T.; Yabushita, H.; Kanaly, R.A.; Shibutani, S.; Yokoyama, A. Increased DNA damage in ALDH2-deficient alcoholics. *Chem. Res. Toxicol.* **2006**, *19*, 1374–1378.
34. Roberts, D.W.; Churchwell, M.I.; Beland, F.A.; Fang, J.L.; Doerge, D.R. Quantitative analysis of etheno-2'-deoxycytidine DNA adducts using on-line immunoaffinity chromatography coupled with LC/ES-MS/MS detection. *Anal. Chem.* **2001**, *73*, 303–309.
35. Raboisson, P; Baurand, A; Cazenave, J.P.; Gachet, C.; Retat, M.; Spiess, B.; Bourguignon, J.J. Novel antagonist sactingat the P2Y(1) purinergicreceptor: Synthesis and conformation alanalysis using potentiometric and nuclear magnetic resonance titration techniques. *J. Med. Chem.* **2002**, *45*, 962–972.
36. Taghizadeh, K.; McFaline, J.L.; Pang, B.; Sullivan, M.; Dong, M.; Plummer, E.; Dedon, P.C. Quantification of DNA damage products resulting from deamination, oxidation and reaction with products of lipid peroxidation by liquid chromatography isotope dilution tandem mass spectrometry. *Nat. Protoc.* **2008**, *3*, 1287–1298.
37. Kasai, H.; Nishimura, S. Hydroxylation of deoxyguanosine at the C-8 position by ascorbic acid and other reducing agents. *Nucleic Acids Res.* **1984**, *12*, 2137–2145.
38. Delaney, J.C.; Essigmann, J.M. Biological properties of single chemical-DNA adducts: A twenty year perspective. *Chem. Res. Toxicol.* **2008**, *21*, 232–252.
39. Cadet, J.; Loft, S.; Olinski, R.; Evans, M.D.; Bialkowski, K.; Richard Wagner, J.; Dedon, P.C.; Møller, P.; Greenberg, M.M.; Cooke, M.S. Biologically relevant oxidants and terminology, classification and nomenclature of oxidatively generated damage to nucleobases and 2-deoxyribose in nucleic acids. *Free Radic. Res.* **2012**, *46*, 367–381.
40. Berquist, B.R.; Wilson, D.M., 3rd. Pathways for repairing and tolerating the spectrum of oxidative DNA lesions. *Cancer Lett.* **2012**, *327*, 61–72.
41. 41Niles, J.C.; Wishnok, J.S.; Tannenbaum, S.R. Peroxynitrite-induced oxidation and nitration products of guanine and 8-oxoguanine: Structures and mechanisms of product formation. *Nitric Oxide* **2006**, *14*, 109–121.
42. Kamiya, H. Mutagenic potentials of damaged nucleic acids produced by reactive oxygen/nitrogen species: Approaches using synthetic oligonucleotides and nucleotides: Survey and summary. *Nucleic Acids Res.* **2003**, *31*, 517–531.
43. Box, H.C.; Budzinski, E.E.; Dawidzik, J.B.; Wallace, J.C.; Iijima, H. Tandem lesions and other products in X-irradiated DNA oligomers. *Radiat. Res.* **1998**, *149*, 433–439.
44. Crean, C.; Uvaydov, Y.; Geacintov, N.E.; Shafirovich, V. Oxidation of single-stranded oligonucleotides by carbonate radical anions: Generating intrastrand cross-links between guanine and thymine bases separated by cytosines. *Nucleic Acids Res.* **2008**, *36*, 742–755.

45. Hong, H.; Cao, H.; Wang, Y.; Wang, Y. Identification and quantification of a guanine-thymine intrastrand cross-link lesion induced by Cu(II)/H_2O_2/ascorbate. *Chem. Res. Toxicol.* **2006**, *19*, 614–621.
46. Nair, J.; Godschalk, R.W.; Nair, U.; Owen, R.W.; Hull, W.E.; Bartsch, H. Identification of 3,N(4)-etheno-5-methyl-2'-deoxycytidine in human DNA: A new modified nucleoside which may perturb genome methylation. *Chem. Res. Toxicol.* **2012**, *25*, 162–169.
47. Knutson, C.G.; Rubinson, E.H.; Akingbade, D.; Anderson, C.S.; Stec, D.F.; Petrova, K.V.; Kozekov, I.D.; Guengerich, F.P.; Rizzo, C.J.; Marnett, L.J. Oxidation and glycolytic cleavage of etheno and propano DNA base adducts. *Biochemistry* **2009**, *48*, 800–809.
48. Otteneder, M.B.; Knutson, C.G.; Daniels, J.S.; Hashim, M.; Crews, B.C.; Remmel, R.P.; Wang, H.; Rizzo, C.; Marnett, L.J. *In vivo* oxidative metabolism of a major peroxidation-derived DNA adduct, M1dG. *Proc. Natl. Acad. Sci. USA* **2006**, *103*, 6665–6669.
49. Wang, H.; Marnett, L.J.; Harris, T.M.; Rizzo, C.J. A novel synthesis of malondialdehyde adducts of deoxyguanosine, deoxyadenosine, and deoxycytidine. *Chem. Res. Toxicol.* **2004**, *17*, 144–149.
50. Minko, I.G.; Kozekov, I.D.; Harris, T.M.; Rizzo, C.J.; Lloyd, R.S.; Stone, M.P. Chemistry and biology of DNA containing 1,N(2)-deoxyguanosine adducts of the alpha,beta-unsaturated aldehydes acrolein, crotonaldehyde, and 4-hydroxynonenal. *Chem. Res. Toxicol.* **2009**, *22*, 759–778.
51. Kawai, Y.; Furuhata, A.; Toyokuni, S.; Aratani, Y.; Uchida, K. Formation of acrolein-derived 2'-deoxyadenosine adduct in an iron-induced carcinogenesis model. *J. Biol. Chem.* **2003**, *278*, 50346–50354.
52. Uchida, K.; Kanematsu, M.; Sakai, K.; Matsuda, T.; Hattori, N.; Mizuno, Y.; Suzuki, D.; Miyata, T.; Noguchi, N.; Niki, E.; *et al.* Protein-bound acrolein: Potential markers for oxidative stress. *Proc. Natl. Acad. Sci. USA* **1998**, *95*, 4882–4887.
53. Liu, X.; Lao, Y.; Yang, I.Y.; Hecht, S.S.; Moriya, M. Replication-coupled repair of crotonaldehyde/acetaldehyde-induced guanine-guanine interstrand cross-links and their mutagenicity. *Biochemistry* **2006**, *45*, 12898–12905.
54. Ishino, K.; Shibata, T.; Ishii, T.; Liu, Y.T.; Toyokuni, S.; Zhu, X.; Sayre, L.M.; Uchida, K. Protein N-acylation: H_2O_2-mediated covalent modification of protein by lipid peroxidation-derived saturated aldehydes. *Chem. Res. Toxicol.* **2008**, *21*, 1261–1270.
55. Eder, E.; Hoffman, C. Identification and characterization of deoxyguanosine adducts of mutagenic beta-alkyl-substituted acrolein congeners. *Chem. Res. Toxicol.* **1993**, *6*, 486–494.
56. Nair, U.; Bartsch, H.; Nair, J. Lipid peroxidation-induced DNA damage in cancer-prone inflammatory diseases: A review of published adduct types and levels in humans. *Free Radic. Biol. Med.* **2007**, *43*, 1109–1120.
57. Blair, I.A. DNA adducts with lipid peroxidation products. *J. Biol. Chem.* **2008**, *283*, 15545–15549.
58. Kasai, H.; Kawai, K. 4-oxo-2-hexenal, a mutagen formed by omega-3 fat peroxidation: Occurrence, detection and adduct formation. *Mutat. Res.* **2008**, *659*, 56–59.
59. Salomon, R.G.; Hong, L.; Hollyfield, J.G. Discovery of carboxyethylpyrroles (CEPs): Critical insights into AMD, autism, cancer, and wound healing from basic research on the chemistry of oxidized phospholipids. *Chem. Res. Toxicol.* **2011**, *24*, 1803–1816.
60. Zhong, W.; Hee, S.Q. Quantitation of normal and formaldehyde-modified deoxynucleosides by high-performance liquid chromatography/UV detection. *Biomed. Chromatogr.* **2004**, *18*, 462–469.

61. Wang, M.; Cheng, G.; Balbo, S.; Carmella, S.G.; Villalta, P.W.; Hecht, S.S. Clear differences in levels of a formaldehyde-DNA adduct in leukocytes of smokers and nonsmokers. *Cancer Res.* **2009**, *69*, 7170–7174.
62. Matsuda, T.; Matsumoto, A.; Uchida, M.; Kanaly, R.A.; Misaki, K.; Shibutani, S.; Kawamoto, T.; Kitagawa, K.; Nakayama, K.I.; Tomokuni, K.; *et al.* Increased formation of hepatic N^2-ethylidene-2'-deoxyguanosine DNA adducts in *aldehyde dehydrogenase 2*-knockout mice treated with ethanol. *Carcinogenesis* **2007**, *28*, 2363–2366.
63. Olsen, R.; Molander, P.; Øvrebø, S.; Ellingsen, D.G.; Thorud, S.; Thomassen, Y.; Lundanes, E.; Greibrokk, T.; Backman, J.; Sjöholm, R.; *et al.* Reaction of glyoxal with 2'-deoxyguanosine, 2'-deoxyadenosine, 2'-deoxycytidine, cytidine, thymidine, and calf thymus DNA: Identification of DNA adducts. *Chem. Res. Toxicol.* **2005**, *18*, 730–739.
64. Frischmann, M.; Bidmon, C.; Angerer, J.; Pischetsrieder, M. Identification of DNA adducts of methylglyoxal. *Chem. Res. Toxicol.* **2005**, *18*, 1586–1592.
65. Masuda, M.; Suzuki, T.; Friesen, M.D.; Ravanat, J.L.; Cadet, J.; Pignatelli, B.; Nishino, H.; Ohshima, H. Chlorination of guanosine and other nucleosides by hypochlorous acid and myeloperoxidase of activated human neutrophils. Catalysis by nicotine and trimethylamine. *J. Biol. Chem.* **2001**, *276*, 40486–40496.
66. Asahi, T.; Kondo, H.; Masuda, M.; Nishino, H.; Aratani, Y.; Naito, Y.; Yoshikawa, T.; Hisaka, S.; Kato, Y.; Osawa, T. Chemical and immunochemical detection of 8-halogenated deoxyguanosines at early stage inflammation. *J. Biol. Chem.* **2010**, *285*, 9282–9291.
67. Byun, J.; Henderson, J.P.; Heinecke, J.W. Identification and quantification of mutagenic halogenated cytosines by gas chromatography, fast atom bombardment, and electrospray ionization tandem mass spectrometry. *Anal. Biochem.* **2003**, *317*, 201–209.

Cancer Science
Japanese Cancer Association JCA
Open Access

Suppressive effects of the NADPH oxidase inhibitor apocynin on intestinal tumorigenesis in obese KK-A^y and *Apc* mutant Min mice

Masami Komiya,[1] Gen Fujii,[2] Shingo Miyamoto,[1] Mami Takahashi,[3] Rikako Ishigamori,[1] Wakana Onuma,[1,4] Kousuke Ishino,[5] Yukari Totsuka,[2] Kyoko Fujimoto[6] and Michihiro Mutoh[1,2]

[1]Epidemiology and Prevention Division, Research Center for Cancer Prevention and Screening, National Cancer Center, Tokyo; Divisions of [2]Carcinogenesis and Cancer Prevention; [3]Central Animal Division, National Cancer Center Research Institute, Tokyo; [4]Faculty of Pharmaceutical Sciences, Tokyo University of Science, Noda-shi; [5]Division of Integrative Oncological Pathology, Nippon Medical School, Tokyo; [6]Division of Molecular Biology, Nagasaki International University, Nagasaki, Japan

Key words

Apc mutant mice, apocynin, iNOS, KK-A^y mice, NADPH oxidase

Correspondence

Michihiro Mutoh, Epidemiology and Prevention Division, Research Center for Cancer Prevention and Screening, National Cancer Center, 5-1-1 Tsukiji, Chuo-ku, Tokyo 104-0045, Japan.
Tel: +81-3-3542-2511, extd 4351; Fax: +81-3-3543-9305;
E-mail: mimutoh@ncc.go.jp

Funding Information

National Cancer Center Research and Development Fund; Ministry of Health, Labor, and Welfare of Japan; Yakult Bio-science Foundation; Japan Agency for Medical Research and Development.

Received April 7, 2015; Revised August 10, 2015; Accepted August 22, 2015

Cancer Sci **106** (2015) 1499–1505

doi: 10.1111/cas.12801

Obesity is a risk factor for colorectal cancer. The accumulation of abdominal fat tissue causes abundant reactive oxygen species production through the activation of NADPH oxidase due to excessive insulin stimulation. The enzyme NADPH oxidase catalyzes the production of reactive oxygen species and evokes the initiation and progression of tumorigenesis. Apocynin is an NADPH oxidase inhibitor that blocks the formation of the NADPH oxidase complex (active form). In this study, we investigated the effects of apocynin on the development of azoxymethane-induced colonic aberrant crypt foci in obese KK-A^y mice and on the development of intestinal polyps in *Apc* mutant Min mice. Six-week-old KK-A^y mice were injected with azoxymethane (200 μg/mouse once per week for 3 weeks) and given 250 mg/L apocynin or 500 mg/L apocynin in their drinking water for 7 weeks. Six-week-old Min mice were also treated with 500 mg/L apocynin for 6 weeks. Treatment with apocynin reduced the number of colorectal aberrant crypt foci in KK-A^y mice by 21% and the number of intestinal polyps in Min mice by 40% compared with untreated mice. Both groups of mice tended to show improved oxidation of serum low-density lipoprotein and 8-oxo-2′-deoxyguanosine adducts in their adipose tissues. In addition, the inducible nitric oxide synthase mRNA levels in polyp tissues decreased. Moreover, apocynin was shown to suppress nuclear factor-κB transcriptional activity *in vitro*. These results suggest that apocynin and other NADPH oxidase inhibitors may be effective colorectal cancer chemopreventive agents.

Obesity is a cause of diabetes mellitus type 2. Insulin resistance induces high levels of fasting glucose, insulin, and IGF1 in the blood. It is now well recognized that individuals with diabetes mellitus type 2 are at high risk for colorectal cancer development.[1,2] The factors that have been suggested to link diabetes mellitus type 2 with colorectal cancer development include hyperinsulinemia, high levels of IGF1 that accelerate cell viability and proliferation,[3] and the dysregulated production of ROS and inflammatory cytokines.[4] It has been shown that insulin activates NADPH oxidase, which produces superoxide and H_2O_2.[5,6]

Phagocyte-derived NADPH oxidase is a well-known ROS-producing enzyme that acts against bacterial infection and inflammation.[7,8] Additional non-phagocyte-derived NADPH oxidase homologs belong to the Duox family. There are seven isoforms in mammals: Nox1, Nox2, Nox3, Nox4, Nox5, Duox1, and Duox2.[9] Nox1, Nox2, Nox4, and Nox5 are expressed in the endothelium, vascular smooth muscle cells, fibroblasts, or perivascular adipocytes. Nox1 is mainly expressed in differentiated colonic epithelial cells.[10,11] Additional homologs have not been identified or are expressed at such low levels that their roles have not been established. Interestingly, Nox/Duox members have been reported to be involved in cancer development. Nox1 stimulates mitogenesis, cell transformation and tumorigenesis when ectopically expressed in NIH3T3 fibroblasts and DU-145 prostate epithelial cells.[12] The overexpression of Nox1 has been observed in prostate, breast, ovarian, and colon cancers.[13–15] Nox1 is overexpressed in human colon cancers and has been correlated with activating mutations in *K-ras*.[16] In Nox1 homozygous knockout mice, the implantation of tumorigenic B16F0 melanoma cells has been observed to result in smaller and less-vascularized implanted tumors. This reduction is associated with the reduced expression levels of several genes, including *VEGF*, *MMP-2*, *MMP-9*, and *NF-κB*.[17] Thus, it is assumed that NADPH oxidase inhibitors may inhibit intestinal tumorigenesis by hindering ROS production and NF-κB activation.

To transport electrons across membranes for the production of superoxides, the Nox/Duox family proteins must form a complex. The catalytic transmembrane protein Nox1 forms a complex with $p22^{phox}$ and the cytoplasmic subunits $p67^{phox}$/NOXO1, $p47^{phox}$/NOXA1, $p40^{phox}$, and Rac1/2. Apocynin,

which belongs to the methoxy-substituted catechol family, effectively inhibits NADPH oxidase activity by blocking the formation of the NADPH oxidase complex; thus, it is used as a standard NADPH oxidase inhibitor in experimental research.[9]

In this study, we show the suppressive effects of apocynin on the number of AOM-induced colorectal aberrant crypt foci (ACF) in obese KK-A^y mice and on intestinal polyp development in Min mice. Min mice have been reported to show high levels of oxidative stress.[18] We showed that the suppressive effects of apocynin treatment on intestinal polyp formation in Min mice were partly explained by the suppression of iNOS. Moreover, apocynin was shown to suppress NF-κB transcriptional activity *in vitro*.

Materials and Methods

Cell culture and chemicals. A human colon cancer cell line (SW48; ATCC, Manassas, VA, USA) and a murine macrophage cell line (RAW264; Riken Cell Bank, Tsukuba, Japan), were cultured in DMEM and RPMI-1640, respectively, containing 10% FBS (HyClone Laboratories, Logan, UT, USA) and antibiotics at 37°C in a humidified incubator at 5% CO_2. The apocynin, 1-(4-hydroxy-3-methoxyphenyl) ethanone, was purchased from Sigma-Aldrich (SAFC, Buchs, Switzerland).

Animals and chemicals. Female 5-week-old KK-A^y/TaJcl (KK-A^y) mice were purchased from Clea Japan (Tokyo, Japan). Male 5-week-old C57BL/6J-$Apc^{Min/+}$ mice (Min mice) were purchased from The Jackson Laboratory (Bar Harbor, ME, USA) and genotyped according to The Jackson Laboratory's protocol. Heterozygotes of the Min strain and wild-type (C57BL/6J) mice were acclimated to laboratory conditions for 1 week. Four to five mice were housed per plastic cage with sterilized softwood chips as bedding in a barrier-sustained animal room at 24 ± 2°C and 55% humidity on a 12:12 h light : dark cycle. The apocynin was well dissolved in drinking water at a concentration of 250 mg/L or 500 mg/L.[19]

Animal experiments. Food and water were available *ad libitum*. The clinical characteristics and mortality rates of the animals were observed daily. The body weights and food consumption rates were measured weekly. For the induction of ACF by AOM (Sigma-Aldrich), 6-week-old female KK-A^y (n = 12) mice were given i.p. injections of AOM (200 μg /mouse) once a week for 3 weeks and 250 mg/L apocynin or 500 mg/L apocynin in their drinking water for 7 weeks. At the end of the experimental period, a blood sample was collected from the abdominal vein and the colorectum was removed, opened longitudinally, and fixed flat between sheets of filter paper in 10% buffered formalin for over 24 h. The colorectum was divided into proximal and rectal segments (1.5 cm in length), and the remainder was divided into proximal (middle) and distal halves. These colorectal sections were stained with 0.2% methylene blue (Merck, Darmstadt, Germany) and PBS, and the mucosal surfaces were assessed for ACF with a stereoscopic microscope as previously reported.[20]

To investigate the effects of apocynin on intestinal tumor formation, seven male 6-week-old Min mice were given 500 mg/L apocynin in their drinking water for 6 weeks, and eight male Min mice without apocynin treatment were used as the control. The intestinal tract was removed and separated into the small intestine, cecum, and colon. The small intestine was first divided to produce a proximal segment (4 cm in length), and the remainder was split into proximal (middle) and distal halves. The tumors in the proximal segment were counted, all tumors were picked up under a stereoscopic microscope, and the remaining intestinal mucosae (non-tumor mucosal portions) were removed by scraping. They were then both stored at −80°C for further analyses using real-time PCR. Additional segments were opened longitudinally and fixed flat between sheets of filter paper in 10% buffered formalin. The numbers and sizes of the tumors and their distributions in the intestines were assessed with a stereoscopic microscope. A portion of the liver, visceral fat, and kidneys were placed into 10% buffered formalin, and liver and visceral fat residues were frozen using liquid nitrogen and stored at −80°C. The experiments were carried out according to the Guidelines for Animal Experiments of the National Cancer Center (Tokyo, Japan) and were approved by the Institutional Ethics Review Committee for Animal Experimentation of the National Cancer Center.

Measurements of mouse serum lipid levels in mice. The serum levels of triglycerides, total cholesterol, and LDL were measured as reported previously.[21] Mouse serum oxLDL levels were measured using an ELISA kit (USCN Life Science, Hubei, China) according to the manufacturer's protocol.

Quantification of 8-oxo-dG using LC-MS/MS. Mouse adipose tissue DNA (from 100 mg tissue) was extracted using the QIAamp DNA Isolation Kit (Qiagen, Hilden, Germany) according to the manufacturer's instructions with minor modifications; deferoxamine mesylate (final concentration, 0.1 mM; Sigma-Aldrich) was added to all samples to prevent the formation of artifactual oxidative adducts during the purification steps. The extracted DNA was dissolved in 25 μL distilled water and stored at −80°C for further analyses. DNA concentration and quality were determined using the NanoDrop ND-1000 spectrometer (Thermo Fisher Scientific, Wilmington, DE, USA). $^{15}N_5$-8-oxo-dG was added to the DNA solutions prior to enzymatic digestion at a concentration of 1.02 nM. The enzymatic digestion conditions were as follows: DNA (2.6–7.0 μg) samples in 5 mM Tris-HCl buffer (pH 7.4) were incubated with DNase I for 3 h. Next, nuclease P1, 10 mM sodium acetate (pH 5.3; final concentration, 10 mM), and $ZnCl_2$ (final concentration, 34 mM) were added, and the samples were incubated for an additional 3 h at 37°C. Finally, alkaline phosphatase, phosphodiesterase I, and Tris base (final concentration, 15.4 mM) were added, and the samples were incubated for 18 h at 37°C. The samples were purified using Vivacon 500 (10-kDa molecular weight cut-off filters Sartorius, Goettingen, Germany), and 15 μL of each of the flow-through fractions was subjected to LC-MS/MS. 8-Oxo-7,8-dihydro-2′-deoxyguanosine and its internal standard were quantified by LC-MS/MS. Positive ions were acquired in the multiple reaction monitoring mode. Multiple reaction monitoring transitions were monitored; the cone voltages and collision energies used were as follows: 8-oxo-dG, [284→168, 35 V, 14 eV], and $^{15}N_5$-8-oxodG, [289→173, 35 V, 14 eV]. The $^{15}N_5$-8-oxo-dG levels were normalized to the DNA concentrations.

Immunohistochemical staining. The small intestines of Min mice with intestinal polyps were fixed, embedded and then sectioned for further immunohistochemical examinations using the avidin–biotin complex immunoperoxidase technique with mouse monoclonal IgG anti-PCNA and anti-cyclin D1 antibodies (Merck Millipore, Billerica, MA, USA) at a 200 × and 100 × dilution, respectively. As the secondary antibody, biotinylated horse anti-rabbit IgG affinity-purified antibody was used at a 200 × dilution. Staining was carried out using avidin–biotin reagents (Vectastain ABC reagents; Vector

Table 1. Development of colorectal aberrant crypt foci (ACF) in KK-A^y mice treated with azoxymethane and apocynin

Apocynin, mg/L	No. of mice with ACF	No. of ACF/colorectum					Mean no. of AC/focus
		Proximal	Middle	Distal	Rectum	Total	
0	12/12	1.1 ± 1.5	16.9 ± 4.8	38.0 ± 10.0	14.5 ± 8.3	70.5 ± 17.2	1.3 ± 0.1
250	12/12	0.3 ± 0.7	7.8 ± 5.9**	28.0 ± 10.9*	12.1 ± 6.3	48.3 ± 20.6**	1.2 ± 0.1
500	12/12	0.2 ± 0.6	10.8 ± 9.8	32.6 ± 12.8	12.1 ± 4.7	55.8 ± 22.3	1.3 ± 0.1

*$P < 0.05$, **$P < 0.01$ *versus* 0 mg/L. Data are expressed as mean ± SD. AC, aberrant crypt.

Table 2. Number of intestinal tumors in Min mice treated with apocynin

Apocynin, mg/L	No. of mice	No. of tumors/mouse				
		Small intestine			Colon	Total
		Proximal	Middle	Distal		
0	8	3.0 ± 0.6	12.1 ± 2.1	34.1 ± 4.6	1.1 ± 0.4	50.4 ± 6.1
500	7	2.6 ± 0.6	8.0 ± 1.7	19.7 ± 1.3*	0.3 ± 0.8	30.6 ± 3.3*

*$P < 0.05$ *versus* 0 mg/L. Data are mean ± SD.

Laboratories, Inc. Burlingame, CA, USA), 3,3′-diaminobenzidine (Sigma-Aldrich), and hydrogen peroxide, and the sections were counterstained with hematoxylin to facilitate orientation. As a negative control, consecutive sections were immunostained without exposure to the primary antibody. The ratio of PCNA-positive cells was calculated by the formula: % = number of PCNA positive cells in polyp / number of whole cells in polyp (magnification, ×100).

Real-time PCR analysis. The tissue samples from the intestinal mucosae or from the polyps of the mice were rapidly deep-frozen in liquid nitrogen and stored at −80°C. Total RNA was isolated from the tissues using TRIzol reagent (Sigma-Aldrich), and 1 μg aliquots in final volumes of 10 μL were used for the synthesis of cDNA using the High Capacity cDNA Reverse Transcription Kit (Applied Biosystems, Foster City, CA, USA). Real-time PCR was carried out using the CFX96 thermal cycler (Bio-Rad, Hercules, CA, USA) with the FastStart Universal SYBR Green Mix (2 ×) (Roche, Basel, Switzerland) according to the manufacturer's instructions. The primers used included mouse c-Myc (5′-GCTCGCCCAAATC CTGTACCT and 3′-TCTCCACAGACACCACATCAATTTC), cyclin D1 (5′-CCATGGAACACCAGCTCCTG and 3′-CGGTC CAGGTAGTTCATGGC), GAPDH (5′-TGTCAGCAATGCAT CCTGCA and 3′-TTACTCCTTGGAGGCCATGT), iNOS (5′-CCGGCAAACCCAAGGTCTACGTT and 3′-CACATCCCGA GCCATGCGCACAT), Nox1 (5′-TCCCTTTGCTTCCTTCTTG A and 3′-CCAGCCAGTGAGGAAGAGTC), $p22^{phox}$ (5′-CGT GGCTACTGCTGGACGTT and 3′-TGGACCCCTTTTTCCTC TTT), and Pai-1 (5′-GACACCCTCAGCATGTTCATC and 3′-AGGGTTGCACTAAACATGTCAG). Cycling conditions were as follows: 95°C for 15 s, annealing at 60°C for 10 s, and 42 cycles at 72°C for 20 s after an initial step of 95°C for 10 min followed by a final elongation step at 72°C for 5 s. To assess the specificity of each primer set, melting curves were constructed for the amplicons generated by the PCR.

Luciferase assay of NF-κB transcriptional activity. To measure NF-κB transcriptional activity, the colon cancer cell line SW48 and rodent macrophage cell line RAW264 were seeded in 96-well plates (2×10^4 cells/well). After 24 h of incubation, the cells were transiently transfected with 100 ng/well of the pGL4.32 (*luc2P*/NF-κB RE/Hygro) (Promega, Madison, WI, USA) reporter plasmid and pGL4.73 (*hRluc*/SV40) (Promega) control plasmid using the FuGENE 6 Transfection Reagent (Roche) according to the manufacturer's instructions and cultured for 24 h. The cells were then treated with 200 μM apocynin for 24 h and, finally, firefly luciferase and Renilla luciferase activities were determined by the Luciferase Assay Systems and Renilla Luciferase Assay Systems (Promega), respectively. The values were normalized according to Renilla luciferase activity levels. The basal luciferase activity of the untreated cells was set as 1.0. The percent of luciferase activity for each treatment was calculated using data from triplicate wells.

Statistical analysis. Statistical analysis was carried out using Student's *t*-test. Differences were considered to be statistically significant at $P < 0.05$.

Results

Suppression of AOM-induced colorectal ACF in KK-A^y mice by apocynin. To determine the effects of apocynin on colorectal ACF development in KK-A^y mice, the KK-A^y mice were treated with AOM, with or without apocynin. Treatment with apocynin did not significantly change the food intake rates, behaviors, or body weights of the mice during the experimental period. The final body weights of the untreated 13-week-old female KK-A^y mice and those that were treated with 250 mg/L apocynin and 500 mg/L apocynin were 49.1 ± 3.3, 47.9 ± 2.4, and 45.0 ± 8.5 g, respectively. During the experimental period, no significant differences in body weights were observed between the groups.

Table 1 shows the numbers and distributions of colorectal ACF in the KK-A^y mice treated with or without apocynin. All KK-A^y mice treated with AOM developed colorectal ACF at 13 weeks. The total number of ACF in the group treated with 250 mg/L apocynin was reduced to 68.5% ($P < 0.01$) of the control value. The numbers of ACF in the middle and distal portions of the colons of the mice treated with 250 mg/L apocynin were reduced significantly ($P < 0.01$, 0.05). There were no significant differences in the number of aberrant crypts per focus between the groups. However, treatment with

250 mg/L apocynin reduced the numbers of small-sized ACF (Fig. S1A).

Suppression of intestinal polyp formation in Min mice by apocynin treatment. Treatment of Min mice with 500 mg/L apocynin for 6 weeks also did not alter body weights, food intake rates, or clinical signs compared with the untreated mice throughout the experimental period. Table 2 summarizes the numbers and distributions of intestinal tumors in the untreated control group and 500 mg/L apocynin-treated group. Almost all tumors developed in the small intestine, with only a few forming in the colon. Treatment with 500 mg/L apocynin led to a decrease in the total number of tumors to 60.7% ($P < 0.05$) of the untreated control value. The total number of tumors in the distal segment decreased by 42.2% in the apocynin group. The majority of tumors were observed to be between 0.5 and 3.0 mm in diameter. Treatment with 500 mg/L apocynin reduced the numbers of tumors of most sizes and significantly reduced the numbers of tumors that were 1.0–1.5 mm in size (Fig. S1B).

To investigate the effects of apocynin on intestinal epithelial cell growth, the intestinal tumor sections of Min mice were

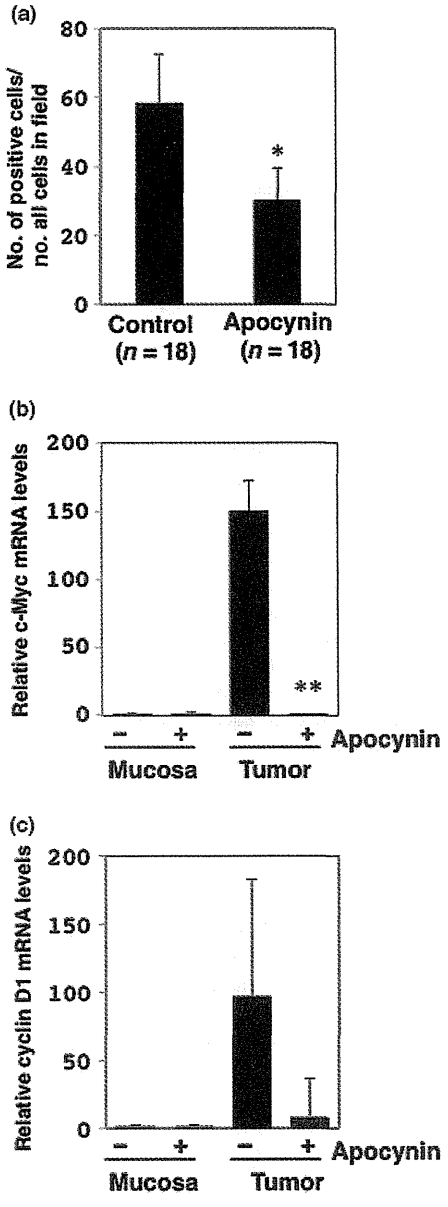

Fig. 1. Changes in cell cycle-related factors in intestinal tumors treated with or without apocynin. (a) Immunohistochemistry was performed for determination of proliferating cell nuclear antigen (PCNA)-positive cell numbers in tumor sections ($n = 18$) of small intestines of Min mice treated with 500 mg/L apocynin ($n = 7$) and untreated controls ($n = 8$). Ratio of the number of PCNA-positive cells per whole cell in field (100 ×) is shown. Data are represented by mean ± SD. *$P < 0.05$ *versus* untreated control. Real-time PCR analysis was carried out to obtain c-Myc (b) and cyclin D1 (c) mRNA levels. Values were set at 1.0 in untreated controls, and relative levels were expressed as mean ± SD ($n = 4$, a pair of mucosa and tumor samples for apocynin or untreated controls). **$P < 0.01$ *versus* untreated control. GAPDH mRNA levels were used to normalize data.

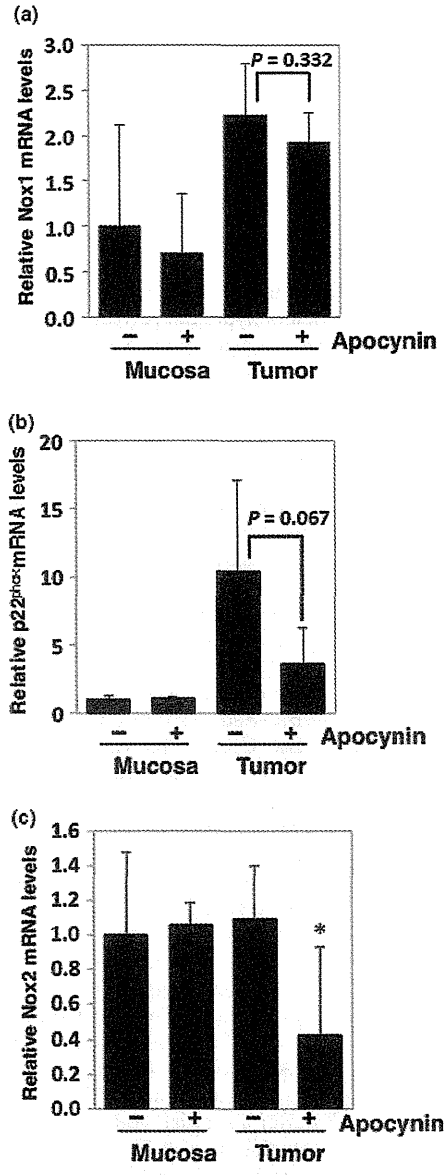

Fig. 2. Relative expression levels of NADPH oxidase-associated genes in intestinal mucosae and tumors of Min mice. Real-time PCR analysis was used to obtain Nox1 (a), $p22^{phox}$ (b), and Nox2 (c) mRNA expression levels. Values were set at 1.0 in untreated controls, and relative levels were expressed as mean ± SD ($n = 4$, a pair of mucosa and tumor samples for apocynin or untreated controls). *$P < 0.05$ *versus* untreated control. GAPDH mRNA levels were used to normalize data.

immunohistochemically stained with anti-PCNA antibody. The proportions of PCNA-positive cells in the intestinal tumor sections significantly decreased by 48.2% in the mice treated with 500 mg/L apocynin ($P < 0.05$) (Fig. 1a). Immunohistopathological analysis for cyclin D1 in intestinal tumors in Min mice also showed a significant decrease of cyclin D1-positive cells in the intestinal tumor sections (Fig. S2). To assess the mechanisms underlying the inhibition of cell growth by apocynin, several cell growth-related genes were analyzed by real-time PCR. The downregulation of the expression levels of c-Myc and cyclin D1 in the small intestinal tumors of Min mice were apparent compared with those of the untreated group (Fig. 1b,c).

Suppressive effects of apocynin on oxidative stress in mice. To clarify the suppression of ROS production by NADPH oxidase inhibition, we examined the effects of apocynin on serum oxLDL-cholesterol levels in the KK-A^y and Min mice. The treatment of the KK-A^y mice with 250 mg/L apocynin significantly suppressed serum oxLDL-cholesterol levels (Table S1). The suppression of serum oxLDL-cholesterol levels was observed in KK-A^y and Min mice at a dose of 500 mg/L apocynin, although the results were not statistically significant (Table S2). Moreover, serum triglyceride, total cholesterol, and LDL-cholesterol levels were measured to assess their effects on the oxLDL-cholesterol levels. The apocynin treatments did not show the serum triglyceride, total cholesterol, or LDL-cholesterol levels to decrease in a dose-dependent manner (Tables S1,S2) in KK-A^y mice; decreases were only observed in Min mice.

To evaluate whether treatment with apocynin improved the oxidative status in other parameters, DNA was extracted from the adipose tissues of both KK-A^y and Min mice, and 8-oxo-dG adducts were quantified per nucleoside by LC-MS/MS. The 8-oxo-dG levels in the adipose tissues of KK-A^y and Min mice tended to decrease following the 500 mg/L apocynin treatment (Fig. S3).

Suppression of iNOS mRNA levels in intestinal tumor sections from Min mice treated with apocynin. To confirm the expression levels of the target molecules of apocynin in Min mice, the levels of NADPH oxidase (Nox1, $p22^{phox}$, and Nox2) mRNA were examined by quantitative RT-PCR. The levels of Nox1 and $p22^{phox}$ increased by 2.2-fold and 10.4-fold, respectively, in the intestinal tumor sections compared with those of the non-tumor mucosal sections in Min mice (Fig. 2a,b). However, the expression levels of Nox2 did not differ between the normal mucosal and tumor sections (Fig. 2c). Nox1, $p22^{phox}$, and Nox2 mRNA levels decreased by 14.3%, 61.2%, and 65.0%, respectively, in the tumor sections following treatment with 500 mg/L apocynin compared with the untreated group (Fig. 2).

Intestinal epithelial cell growth is generally affected by inflammation-related factors, including cytokines and growth factors. Thus, we next focused on the expression levels of interleukin-6, iNOS, and Pai-1 in the intestinal tissues. In the tumor sections, the Pai-1 and iNOS mRNA levels were upregulated compared with the levels observed in the non-tumor mucosal sections, and these levels decreased following 500 mg/L apocynin treatment (Fig. 3a,b). However, interleukin-6 mRNA levels decreased only in the non-tumor mucosal sections following apocynin treatment (Fig. 3c).

Nuclear factor-κB transcription is inhibited by apocynin treatment. To examine the effects of apocynin on the transcriptional factors that regulate the expression of iNOS, we examined NF-κB transcriptional activity in SW48 (human colon cancer cell line) and RAW264 (murine macrophage cell line) cells. The NF-κB transcriptional activities in both cell lines were reduced by 24 h of 200 μM apocynin treatment (Fig. 4).

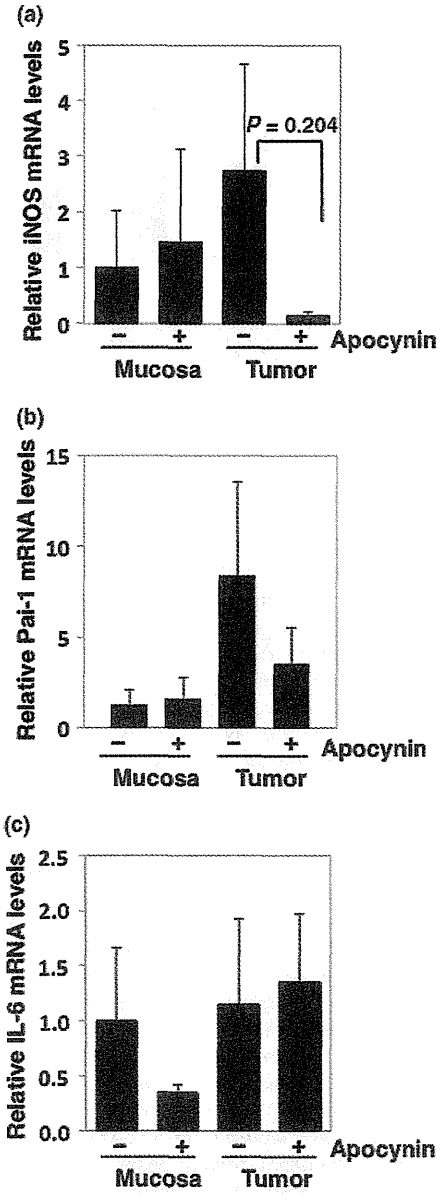

Fig. 3. Relative expression levels of inflammation- and carcinogenesis-related genes in intestinal mucosae and tumors of Min mice treated with or without 500 mg/L apocynin. Real-time PCR analysis was carried out to obtain iNOS (a), Pai-1 (b), and interleukin-6 (IL-6) (c) mRNA levels. Values were set at 1.0 in untreated controls, and relative levels were expressed as mean ± SD ($n = 4$, a pair of mucosa and tumor samples for apocynin or untreated controls). GAPDH mRNA levels were used to normalize data.

Discussion

In the present study, we showed the suppressive effects of apocynin on AOM-induced colorectal ACF formation in obese KK-A^y mice and on intestinal tumor development in Min mice. Moreover, the clear suppression of c-Myc and cyclin D1 mRNA levels and a reduced ratio of PCNA-positive epithelial

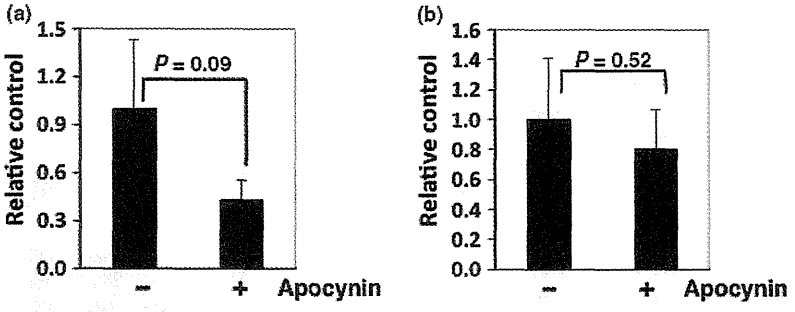

Fig. 4. Nuclear factor-κB (NF-κB) transcriptional activity levels in human colon cancer cells and rodent macrophage cells. SW48 (a) and RAW264 (b) cells were seeded in 96-well plates (2×10^4 cells/well) and were transiently transfected with pGL4.32 (*luc2P*/NF-κB RE/Hygro) reporter plasmid and pGL4.73 (*hRluc*/SV40) control plasmid for 24 h. Cells were then treated with 200 μM apocynin for 24 h, and firefly luciferase and Renilla luciferase activities were determined by luciferase assay systems and Renilla luciferase assay systems, respectively. Basal luciferase activity of untreated cells was set at 1.0. Percentage of luciferase activity was calculated from data obtained from triplicate wells for each treatment. Values were normalized by Renilla luciferase activity levels. Data are expressed as mean ± SD ($n = 3$).

cells were observed in the intestinal tumor sections of Min mice. Treatment with apocynin tended to decrease levels of oxidative stress in both KK-A^y and Min mice. The mechanism involved in the suppressive effects of apocynin treatment on oxidative stress was partially related to the inhibition of NADPH oxidase, resulting in reduced ROS production, and the suppression of iNOS mRNA levels. In addition, the reporter gene assay revealed that apocynin inhibited NF-κB transcriptional activity in human colon cancer cells.

It has been reported that Nox1 knockdown induces G_0/G_1 arrest in a human colon cell line, HT29, whereas the same knockdown treatment in Caco2 cells strongly induces apoptosis.[22] In addition, apocynin also blocks cell growth by inducing G_0/G_1 arrest and downregulating cyclin D1 in a human prostate cancer cell line, LNCaP.[19] We obtained similar results, showing that apocynin suppressed c-Myc and cyclin D1 mRNA levels and reduced the ratio of PCNA-positive epithelial cells in the intestinal polyp sections of Min mice. This inhibition of cell growth factors may result in a reduction in AOM-induced colorectal ACF formation in obese KK-A^y mice and intestinal tumor development in Min mice.

Because apocynin is known to be an NADPH oxidase inhibitor, we examined ROS activity by measuring serum oxLDL levels, and the number of 8-oxo-dG adducts per nucleoside in the adipose tissue was quantified by LC-MS/MS. Both assessments indicated a tendency toward reduction by the apocynin treatment. Compared with other serum lipids, serum oxLDL levels were not affected by the amount of total serum cholesterol or LDL. Because ROS are generally produced by mitochondria and peroxisomes and the enzymes cytochrome P450 and NADPH oxidase,[9,23,24] the targeting of only NADPH oxidase does not sufficiently reduce whole-body ROS production. We speculated that apocynin did not affect whole-body ROS production, but may play an important role in the local tumor parts of the intestine in which NADPH oxidase is overexpressed. Neoplastic lesions with characteristically elevated levels of NADPH oxidase, such as human colon adenomas and well-differentiated adenocarcinomas,[15] may be good targets for NADPH oxidase inhibitors.

The present study is the first to show that *Nox1* and *p22^{phox}* mRNA levels tend to be elevated in the intestinal tumors of Min mice. It has been reported that PhIP-induced colon tumors show increased Nox1 expression and NF-κB activation.[22] PhIP is a heterocyclic amine that has been associated with colon cancer in rodents. In addition, our results imply that increased Nox/Duox expression is not specific to heterocyclic amines or to other colon carcinogens, such as AOM. It has been reported that Nox1 overexpression in human colon cancers correlate with activating mutations in *K-ras*.[16] However, considering that genetic alterations in β-*catenin* or *APC* have been detected in over 80% of human colorectal cancers and that Min mice possessed *Apc* mutations in this study, β-catenin signaling may also be influenced by the expression of Nox1. Further research is needed to confirm this possibility.

Reactive oxygen species affect cancer cell proliferation through the activation of NF-κB transcription factors,[25] which results in the induction of cyclin D1 and cyclin-dependent kinase. Moreover, NF-κB induces inflammatory cytokines, growth factors, and inflammation-related enzymes, such as iNOS. In cultured rodent macrophage cells and human colon cancer cells, apocynin has been shown to inhibit NF-κB transcriptional activity in this study. Decreased production of intracellular ROS by apocynin could be involved in the inhibition of NF-κB transcriptional activity. Moreover, inhibition of Akt phosphorylation by apocynin[26] could partly inhibit NF-κB transcriptional activity through IKK activation. These mechanisms may partially explain the lowered expression levels of c-Myc, cyclin D1, and iNOS, which are downstream targets of NF-κB, observed in the intestinal polyps of Min mice in this study.

In summary, we have provided the first evidence of the involvement of Nox/Duox in AOM-induced colon carcinogenesis in obese mice and in intestinal tumor formation in Min mice using an NADPH oxidase inhibitor, apocynin. The chemopreventive effect of apocynin on non-obese ordinary mice is another concern. Although Min mice are not obese mice, AOM-induced non-obese ordinary mouse colorectal cancer will be a more suitable model to demonstrate the effect of apocynin on carcinogenesis in non-obese ordinary mice. In addition, clarifying the correlation between Nox/Duox family members and NF-κB–iNOS during colon cancer development warrants further investigation. We conclude that apocynin and other NADPH oxidase inhibitors may be effective colorectal cancer chemopreventive agents. Further evidence, such as that obtained from human trials, is required.

Acknowledgments

We received technical support from Ms. Shimura M. We thank Mr. Uchiya N. and the National Cancer Center Research Core Facility for some of the analyses performed in this study. The Core Facility was supported by the National Cancer Center Research and Development Fund (23-A-7). This work was

supported by Grants-in-Aid for Cancer Research, the Third-Term Comprehensive 10-Year Strategy for Cancer Control from the Ministry of Health, Labor, and Welfare of Japan, and the Yakult Bio-science Foundation, and Practical Research for Innovative Cancer Control from the Japan Agency for Medical Research and Development (15ck0106098h0002).

Disclosure Statement

The authors have no conflicts of interest.

Abbreviations

ACF	aberrant crypt foci
AOM	azoxymethane
IGF	insulin-like growth factor
Duox	dual oxidase
iNOS	inducible nitric oxide synthase
LC-MS/MS	liquid chromatography tandem mass spectrometry
LDL	low-density lipoprotein
NF-κB	nuclear factor-κB
Nox	NADPH oxidase
oxLDL	oxidized LDL
8-oxo-dG	8-oxo-7,8-dihydro-2′-deoxyguanosine
Pai	plasminogen activator inhibitor
PCNA	proliferating cell nuclear antigen
ROS	reactive oxygen species

References

1 Moghaddam AA, Woodward M, Huxley R. Obesity and risk of colorectal cancer: a meta-analysis of 31 studies with 70,000 events. *Cancer Epidemiol Biomarkers Prev* 2007; **16**: 2533–47.
2 Khandekar MJ, Cohen P, Spiegelman BM. Molecular mechanisms of cancer development in obesity. *Nat Rev Cancer* 2011; **11**: 886–95.
3 Ewton DZ, Kansra S, Lim S, Friedman E. Insulin-like growth factor-I has a biphasic effect on colon carcinoma cells through transient inactivation of forkhead1, initially mitogenic then mediating growth arrest and differentiation. *Int J Cancer* 2002; **98**: 665–73.
4 Ishino K, Mutoh M, Totsuka Y, Nakagama H. Metabolic syndrome: a novel high-risk state for colorectal cancer. *Cancer Lett* 2013; **334**: 56–61.
5 Lawrece JC Jr, Larner J. Activation of glycogen synthase in rat adipocytes by insulin and glucose involves increased glucose transport and phosphorylation. *J Biol Chem* 1978; **253**: 2104–13.
6 Mukherjee SP, Lane RH, Lynn WS. Endogenous hydrogen peroxide and peroxidative metabolism in adipocytes in response to insulin and sulfhydryl reagents. *Biochem Pharmacol* 1978; **27**: 2589–94.
7 Gloire G, Legrand-Poels S, Piette J. NF-kappaB activation by reactive oxygen species: fifteen years later. *Biochem Pharmacol* 2006; **72**: 1493–505.
8 Quinn MT, Ammons MC, Deleo FR. The expanding role of NADPH oxidases in health and disease: no longer just agents of death and destruction. *Clin Sci* 2006; **111**: 1–20.
9 Bedard K, Krause KH. The NOX family of ROS-generating NADPH oxidases: physiology and pathophysiology. *Physiol Rev* 2007; **87**: 245–313.
10 Geiszt M, Witta J, Baffi J, Lekstrom K, Leto TL. Dual oxidases represent novel hydrogen peroxide sources supporting mucosal surface host defense. *FASEB J* 2003; **17**: 1502–4.
11 Szanto I, Rubbia-Brandt L, Kiss P *et al.* Expression of NOX1, a superoxide-generating NADPH oxidase, in colon cancer and inflammatory bowel disease. *J Pathol* 2005; **207**: 164–76.
12 Suh YA, Arnold RS, Lassegue B *et al.* Cell transformation by the superoxide-generating oxidase Mox1. *Nature* 1999; **401**: 79–82.
13 Lim SD, Sun C, Lambeth JD *et al.* Increased Nox1 and hydrogen peroxide in prostate cancer. *Prostate* 2005; **62**: 200–7.
14 Desouki MM, Kulawiec M, Bansal S, Das GM, Singh KK. Cross talk between mitochondria and superoxide generating NADPH oxidase in breast and ovarian tumors. *Cancer Biol Ther* 2005; **4**: 1367–73.
15 Fukuyama M, Rokutan K, Sano T, Miyake H, Shimada M, Tashiro S. Overexpression of a novel superoxide-producing enzyme, NADPH oxidase 1, in adenoma and well differentiated adenocarcinoma of the human colon. *Cancer Lett* 2005; **221**: 97–104.
16 Laurent E, McCoy JW 3rd, Macina RA *et al.* Nox1 is over-expressed in human colon cancers and correlates with activating mutation in K-Ras. *Int J Cancer* 2008; **123**: 100–7.
17 Garrido-Urbani S, Ugur T, Schleussner E *et al.* Targeting vascular NADPH oxidase 1 blocks tumor angiogenesis through a PPARα mediated mechanism. *PLoS One* 2011; **6**: e14665.
18 Ikeda K, Mutoh M, Teraoka N, Nakanishi H, Wakabayashi K, Taguchi R. Increase of oxidant-related triglycerides and phosphatidylcholines in serum and small intestinal mucosa during development of intestinal polyp formation in Min mice. *Cancer Sci* 2011; **102**: 79–87.
19 Suzuki S, Shiraga K, Sato S *et al.* Apocynin, an NADPH oxidase inhibitor, suppresses rat prostate carcinogenesis. *Cancer Sci* 2013; **104**: 1711–7.
20 Mutoh M, Watanabe K, Kitamura T *et al.* Involvement of prostaglandin E receptor subtype EP4 in colon carcinogenesis. *Cancer Res* 2002; **62**: 28–32.
21 Usui S, Nakamura M, Jitsukata K, Nara M, Hosaki S, Okazaki M. Assessment of between-instrument variations in a HPLC method for serum lipoproteins and its traceability to reference methods for total cholesterol and HDL-cholesterol. *Clin Chem* 2000; **46**: 63–72.
22 Wang R, Dashwood WM, Nian H *et al.* NADPH oxidase overexpression in human colon cancers and rat colon tumors induced by 2-amino-1-methyl-6-phenylimidazo[4,5-b]pyridine (PhIP). *Int J Cancer* 2011; **128**: 2581–90.
23 Wu WS. The signaling mechanism of ROS in tumor progression. *Cancer Metastasis Rev* 2006; **25**: 695–705.
24 Khandrika L, Kumar B, Koul S, Maroni P, Koul HK. Oxidative stress in prostate cancer. *Cancer Lett* 2009; **282**: 125–36.
25 Sen CK, Packer L. Antioxidant and redox regulation of gene transcription. *FASEB J* 1996; **10**: 709–20.
26 Lirdprapamongkol K, Kramb JP, Suthiphongchai T *et al.* Vanillin suppresses metastatic potential of human cancer cells through PI3K inhibition and decreases angiogenesis in vivo. *J Agric Food Chem* 2009; **57**: 3055–63.

Supporting Information

Additional supporting information may be found in the online version of this article:

Fig. S1. Effect of apocynin on aberrant crypt foci size and intestinal tumor size distribution in the mice.

Fig. S2. Histopathological and immunohistopathological analysis of intestinal tumors in Min mice.

Fig. S3. Oxidative adduct qualification in DNA extracted from adipose tissues of mice. Mouse DNA was extracted from adipose tissues of KK-A^y and Min mice treated with or without 500 mg/L apocynin. The numbers of 8-oxodG adducts per nucleoside were quantified by liquid chromatograph tandam mass spectrometry (LC-MS/MS). Data are expressed as mean ±SD (N=4).

Table S1. Serum lipid levels in KK-A^y mice with or without apocynin treatment.

Table S2. Serum lipid levels in Min mice with or without apocynin treatment.

Mutagenesis Advance Access published December 16, 2015

Mutagenesis, 2015, 00, 1–9
doi:10.1093/mutage/gev076
Original Manuscript

OXFORD

Original Manuscript

Tumour-promoting activity of polycyclic aromatic hydrocarbons and their oxygenated or nitrated derivatives

Kentaro Misaki[1,2,*], Takeji Takamura-Enya[3], Hideoki Ogawa[1], Kenji Takamori[1] and Mitsuaki Yanagida[1]

[1]Institute for Environmental and Gender Specific Medicine, Juntendo University Graduate School of Medicine, 2-1-1 Tomioka, Urayasu, Chiba 279-0021, Japan, [2]School of Nursing, University of Shizuoka, 52-1 Yada, Suruga-ku, Shizuoka 422–8526, Japan and [3]Department of Applied Chemistry, Kanagawa Institute of Technology, 1030 Shimo-Ogino, Atsugi, Kanagawa 243–0292, Japan

*To whom correspondence should be addressed. Tel: +81 54 264 5462; Fax: +81 54 264 5462; Email: kmisaki@u-shizuoka-ken.ac.jp

Received 4 February 2015; Revised 12 October 2015; Accepted 13 October 2015.

Abstract

Various types of polycyclic aromatic compounds (PACs) in diesel exhaust particles are thought to contribute to carcinogenesis in mammals. Although the carcinogenicity, mutagenicity and tumour-initiating activity of these compounds have been evaluated, their tumour-promoting activity is unclear. In the present study, to determine the tumour-inducing activity of PACs, including previously known mutagenic compounds in atmospheric environments, a transformation assay for promoting activity mediated by the release of contact inhibition was conducted for six polycyclic aromatic hydrocarbons (PAHs), seven oxygenated PAHs (oxy-PAHs) and seven nitrated PAHs (nitro-PAHs) using mouse embryonic fibroblast cells transfected with the v-Ha-*ras* gene (Bhas 42 cells). Of these, two PAHs [benzo[*k*]fluoranthene (B[*k*]FA) and benzo[*b*]fluoranthene (B[*b*]FA)], one oxy-PAH [6*H*-benzo[*cd*]pyren-6-one (BPO)] and two nitro-PAHs (3-nitro-7*H*-benz[*de*]anthracen-7-one and 6-nitrochrysene) were found to exhibit particularly powerful tumour-promoting activity (≥10 foci following exposure to <100 nM). In addition, clear mRNA expression of CYP1A1, which is associated with aryl hydrocarbon receptor (AhR)-mediated activation, was observed following the exposure of cells to two PAHs (B[*k*]FA and B[*b*]FA) and three oxy-PAHs (1,2-naphthoquinone, 11*H*-benzo[*b*]fluoren-11-one and BPO). Further, an HO-1 antioxidant response activation was observed following exposure to B[*k*]FA, B[*b*]FA and BPO, suggesting that the induction of tumour-promoting activity in these compounds is correlated with the dysfunction of signal transduction *via* AhR-mediated responses and/or oxidative stress responses.

Introduction

The atmospheric environment contains various types of compounds from exhaust gas and particulate matter emitted from internal combustion engines, such as those in industrial factories, combustion furnaces and automobiles (1,2). Several epidemiological studies have identified an association between diesel exhaust particles (DEPs) and the occurrence of cancers of the lung and other organs (3). DEPs contain various types of polycyclic aromatic compounds (PACs) that are thought to be the principle active factors responsible for the carcinogenicity of DEPs. To date, a large amount of data regarding the mutagenicity, carcinogenicity and DNA adduct formation with PACs have been accumulated (4–8). The United States Environmental Protection Agency (EPA) and the International Agency for Research on Cancer (IARC) have classified polycyclic aromatic hydrocarbons (PAHs) such as benzo[*a*]pyrene (B[*a*]P), benz[*a*]anthracene (B[*a*]A), chrysene (Chr), benzo[*b*]fluoranthene (B[*b*]FA), benzo[*k*]fluoranthene (B[*k*]FA) and dibenzo[*a*,*l*]pyrene (DB[*a*,*l*]P) as carcinogens or probable/possible carcinogens in humans (4,5).

Along with PAHs, oxygenated PAHs (oxy-PAHs), such as polycyclic aromatic quinones and polycyclic aromatic ketones, are present as PACs in atmospheric diesel exhaust and airborne particles (8–12). However, the toxicological significance of these compounds is not well understood (7,13,14). Several studies have reported that polycyclic aromatic quinones induce severe adverse biological effects such as allergic inflammation and disruption of vascular tone *via* induction of the reactive oxygen species (ROS) pathway (15–19).

Nitrated PAHs (nitro-PAHs) are originally emitted from various combustion engines and are more likely to be formed by the reaction of parental compounds with nitrogen dioxide in ambient air (20). Nitro-PAHs are well-known bacterial direct-acting mutagens and carcinogens for mammals (2,6,21,22). Nitro-PAHs, such as 1-nitropyrene (1-NPy), 1,6-dinitropyrene (1,6-DNPy), 1,8-dinitropyrene (1,8-DNPy) and 6-nitrochrysene (6-NChr), have been categorised as probable carcinogens by IARC (5,21). Enya *et al.* identified a new nitrated oxy-PAH, 3-nitro-7*H*-benz[*de*]anthracen-7-one (3-NBAO), as a novel potent mutagenic and carcinogenic compound in the polar fraction of DEPs (23–25), and the compound has been categorised to be a probable carcinogen by IARC (21). Several other mutagenic nitrated oxy-PAHs and normal nitro-PAHs have been reported to possibly contribute to the mutagenic activity of environmental samples (26–28).

Although many studies have reported on the carcinogenic and mutagenic activity of the above-mentioned PACs, studies regarding the tumour-promoting activity of these compounds are limited (29,30). Therefore, the underlying mechanisms promoting these activities have not completely been elucidated. Recently, a simple assay to detect the carcinogenic promoting activities of test compounds was developed by Ohmori *et al.* (31) using mouse embryonic fibroblasts (BALB/3T3 cells) transfected with the v-Ha-*ras* gene (Bhas 42 cells). Using this assay, several PACs, including B[*a*]A, Chr and 1-NPy, were found to have significant tumour-promoting activities. This indicates that other PACs, which have yet to be evaluated, are very likely to show positive responses using this assay (29).

Several compounds are known to promote tumour formation, including ROS-producing compounds such as arsenic compounds, metal (cadmium and zinc) chlorides and catechol, which exhibited tumour-promoting activities as determined by the Bhas 42 assay as well as others (30). Dioxins were also reported to exhibit tumour-promoting activities *via* mechanisms that included cell cycle regulation that correlated with aryl hydrocarbon receptor (AhR)-mediated gene induction activity (32–34). Because several PAHs (35–37), nitro-PAHs (37,38) and polycyclic *o*-quinines(39) are known to promote AhR-mediated gene transcription activities to induce the production of metabolic enzymes such as cytochromes (CYPs), it is plausible that several PACs with high AhR-mediated gene transcription activities have high tumour-promoting activities.

In addition, Misaki *et al.* (40) examined AhR-mediated transcriptional activity induced by several types of oxy-PAHs to promote metabolic enzyme induction and reported for the first time that several oxy-PAHs [i.e. benzo[*b*]fluorenone (B[*b*]FO), benzo[*a*]fluorenone (B[*a*]FO) and naphthacenequinone (NCQ)] had significantly high AhR-mediated transcriptional activities, inducing the cytochrome P450 family 1 gene (CYP1A1) (41). These compounds were also shown to induce antioxidant response element (ARE)-mediated aldo-keto reductase family 1 gene (AKR1C1) (41). Experimental results of the transcriptional activity of these compounds have been supported by numerous published reports of ROS induction by several nitro-PAHs (38,42), quinone compounds (15–19,42) and PAH metabolites (15,38,42).

Taken together, the findings of these previous studies suggest that several PACs with high AhR and/or ROS-inducing activities may be good candidates as tumour-promoting compounds. Therefore, in the present study, a transformation assay with Bhas 42 cells was used to identify the tumour-promoting activities of PACs (six PAHs, seven oxy-PAHs and seven nitro-PAHs) in the atmosphere to test the above-mentioned hypothesis. CYP1A1 mRNA levels induced *via* the AhR system and/or antioxidant signalling [heme oxygenase (HO)-1] of representative compounds were also analysed to determine whether signal transduction is relevant to the tumour-promoting activities of the selected compounds.

Materials and methods

Chemicals

B[*a*]P, Chr and 12-*O*-tetradecanoylphorbol-13-acetate (TPA) were purchased from Wako Pure Chemical Industries, Ltd. (Osaka, Japan). DB[*a*,*l*]P, 3-nitrofluoranthene (3-NFA) and 6-NChr were supplied by AccuStandard, Inc. (New Haven, CT, USA), and 8-nitrofluoranthene (8-NFA) was purchased from Nihon Fine Chemical (Tokyo, Japan). All other test chemicals were obtained from Sigma–Aldrich (St. Louis, MO, USA). The purities of B[*b*]FA, B[*k*]FA, 7,12-benz[*a*]anthracenequinone (BAQ), 1,6-DNPy and 1,8-DNPy were 98%, the purities of B[*a*]P, 1,2-naphthoquinone (NPhQ), NCQ and TPA were 97%, and the purity of 3-NFA was >96%. The purities of the other test chemicals were ≥99%.

B[*a*]FO, B[*b*]FO and 6*H*-benzo[*cd*]pyren-6-one (BPO) were synthesised as described previously (43,44), purified by column chromatography, and then recrystallised. The purities of the synthesised compounds were >99%. The 3-NBAO was prepared by nitration of benzanthrone, as described previously (24).

Minimum essential medium (MEM), Dulbecco's modified Eagle's medium/Ham's F12 (DMEM/F12) and fetal bovine serum (FBS) were purchased from Nissui Pharmaceutical Co., Ltd. (Tokyo, Japan), Life Technologies (Carlsbad, CA, USA) and Hana-Nesco Bio Corp. (Tokyo, Japan), respectively. The RNA extraction reagent was purchased from Qiagen (Valencia, CA, USA). Dimethyl sulfoxide (DMSO) was purchased from Wako Pure Chemical Industries, Ltd.

Bhas 42 cell culture

The mouse fibroblast cell line Bhas 42 was obtained from the Health Science Research Resources Bank (Sennan, Osaka, Japan). The cells were incubated in MEM with 10% (v/v) FBS at 37°C in a humidified atmosphere containing 5% CO_2. The cells were sub-cultured before reaching confluence.

Transformation assay to detect tumour-promoting activity

Tumour-promoting activity was evaluated using a transformation assay, as described previously (29,30). In brief, 4×10^4 Bhas 42 cells in 2 ml of DMEM/F12 with 5% FBS were cultured in each well of six-well microplates (Day 0). The medium was changed with fresh medium containing the test chemicals on Days 3, 7 and 10 after the initial harvest and then treated with only fresh medium on Day 14. On Day 21, the cells were fixed with methanol and stained with 5% Giemsa solution. All the chemicals were dissolved in DMSO and the final concentration of the solvent in the culture medium was 0.1% (v/v). Control cells were treated with 0.1% (v/v) DMSO. Cell cultures were prepared in triplicate for each chemical at each concentration.

The number of foci in each well was based on the morphological criteria used in a previous study (31) as follows: (i) deep basophilicity, (ii) dense multi-layering of cells, (iii) random orientation of cells at the edge of foci and (iv) ≥20 cells within a focus. If a significant increase in focus number with a P value of <0.01 was observed at ≥1 concentration, or a significant increase with a P value of <0.05 was observed at ≥2 serial concentrations by the Dunnett test analysis, the chemical was regarded as positive. If ≥10 foci were confirmed following exposure to <100 nM for a positive chemical, the chemical was regarded as a powerful positive. If a significant increase in focus number with a P value of <0.05 was observed at only one concentration, the chemical was regarded as equivocal. If there was no significant increase in focus number at any concentration, the chemical was regarded as negative.

Cell viability assay

Cell viability in response to each chemical was examined using the 3-(4,5-dimethylthiazol-2-yl)-5-(3-carboxymethoxyphenyl)-2-(4-sulfophenyl)-2*H*-tetrazolium salt (MTS) assay, basically according to the manufacturer's protocol (45). Cells were cultured in each well of 24-well microplates by adjusting the cell numbers to 1×10^4 cells in 500 µl of DMEM/F12 with 5% FBS. On Day 3, the medium was changed to fresh medium containing a test chemical. On Day 7, 100 µl of MTS solution was added to the medium, and after 4 h, optical density at 490 nm was measured using a plate reader (ARVO™ X3; PerkinElmer, Inc., Waltham, MA, USA).

RNA isolation, reverse transcription and real-time polymerase chain reaction

Cells were cultured in each well of six-well microplates by adjusting the cell numbers to 4×10^4 cells in 2 ml of DMEM/F12 with 5% FBS. On Day 3, the cells were treated for 24 h with medium containing a test chemical. On Day 4, total RNA was isolated from the cells using the RNeasy Mini Kit (Qiagen) and DNA-Free™ Kit (Applied Biosystems, Foster City, CA, USA), according to the manufacturers' protocols. Total RNA was dissolved in RNase-free water and the concentration was determined spectrometrically. Cell cultures were prepared in triplicate for each chemical.

Total RNA (100 ng) was added to a reaction mixture containing 100 pmol of random hexamers, Prime Script® RT Enzyme Mix and deoxyribonucleoside triphosphates in a final volume of 20 µl and reverse transcribed using the Prime Script® RT Reagent Kit (Perfect Real Time) (Takara Bio, Inc., Otsu, Japan). The reaction mixture was incubated at 37°C for 15 min and heated at 85°C for 5 min to inactivate the enzyme according to the manufacturer's protocol.

The following previously reported oligonucleotides used for polymerase chain reaction (PCR) were commercially synthesised by Sigma–Aldrich Japan (Ishikari, Japan) (46–48):

- 18S rRNA: 5′-TTGACGGAAGGGCACCACCAG-3′ (130 bp)
  5′-GCACCACCACCCACGGAATCG-3′
- CYP1A1: 5′-CCTCTTTGGAGCTGGGTTTG-3′ (230 bp)
  5′-TGCTGTGGGGGATGGTGAAG-3′
- HO-1: 5′-TCAGGTGTCCAGAGAAGGCTTT-3′ (70 bp)
  5′-CTCTTCCAGGGCCGTGTAGA-3′

Quantification of cDNA was performed using the ABI PRISM 7900HT Sequence Detection System (Applied Biosystems), and staining was performed with SYBR Green I. A 2 µl aliquot of the reverse transcription (RT) mixture was added to a PCR mixture containing 0.2 µM of each primer and SYBR® Premix Ex Taq DNA polymerase in a final volume of 25 µl and amplified using the SYBR® Premix Ex Taq™ Kit (Perfect Real Time) (Takara Bio, Inc.) according to the manufacturer's protocol. The PCR reactions were performed with 1 cycle at 95°C for 30 s and 40 cycles of 95°C for 5 s and 65°C for 30 s. The specificity of the PCR products was determined by a melting curve analysis and expression levels were normalised against 18S rRNA levels. A significant increase ($P < 0.05$) of fold induction, namely the ratio of the normalised value in PAC-treated cells divided by the value in DMSO control cells, was evaluated using the Student's t-test.

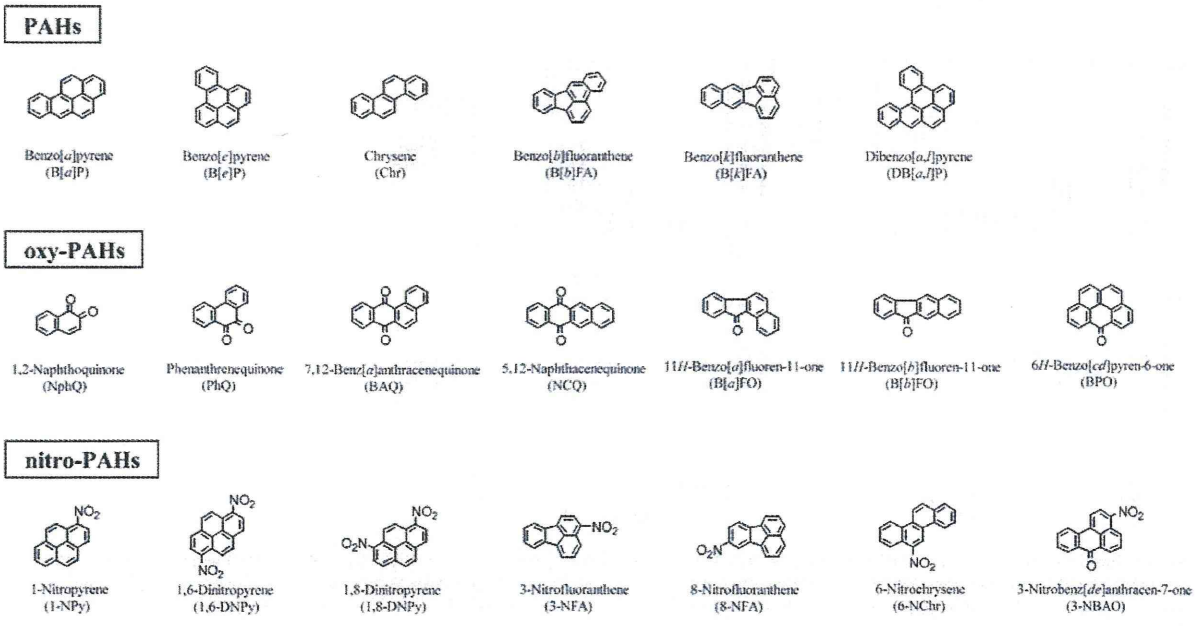

Figure 1. PAHs, oxy-PAHs and nitro-PAHs examined in the present study.

Results

Tumour-promoting activities of PACs

In the present study, a transformation assay to evaluate tumour-promoting activity using Bhas 42 cells was performed for 6 PAHs, 7 oxy-PAHs and 7 nitro-PAHs, which exist in DEPs (Figure 1). The tumour-promoting activity was statistically significant ($P < 0.05$) when ≥8 foci were detected. The representative promoter TPA significantly increased the number of foci within the range of 8–160 nM (Figure 2). Using the same system, two PAHs (i.e. B[*k*]FA and B[*b*]FA) and one oxy-PAH (BPO) were powerfully positive having particularly high tumour-promoting activities (Figure 2A and E, respectively). All nitro-PAHs tested exhibited at least eight foci at 200 nM. Among them, 3-NBAO and 6-NChr demonstrated the most powerful transformation activities (Figure 2G and I, respectively). The order of the strength of tumour-promoting activities among the oxy-PAHs to induce ≥8 foci, as judged from the lowest concentration and obtained from the dose–response curve, was BPO > B[*b*]FO, NphQ > B[*a*]FO, BAQ > NCQ (Figure 2C and E). The order of the strength among nitro-PAHs was 3-NBAO, 6-NChr > 1,6-DNPy, 1,8-DNPy, 8-NFA > 3-NFA > 1-NPy (Figure 2G and I). For the PACs, the tumour-promoting activity of Chr was considered medium while that of 1-NPy and benzo[*e*]pyrene (B[*e*]P) was low (Figure 2A and G), confirming the results of a previous study (29). The activity of B[*a*]P was not significant in this assay (Figure 2A), although the activity was reported as equivocal (29). No tumour-promoting activities could be detected for DB[*a*,*l*]P and phenanthrenequinone (PhQ) (Figure 2A and C). In an MTS assay, DB[*a*,*l*]P, PhQ, NphQ, 6-NChr and 3-NBAO exhibited a markedly greater decrease in cell viability (Figure 2B, D and J).

Induction of mRNA of metabolic enzymes after exposure to PAHs and oxy-PAHs

To investigate the molecular mechanisms of tumour-promoting activity, we analysed the amounts of CYP1A1 and HO-1 mRNA in Bhas 42 cells induced with representative active compounds by 24 h incubations (the time point predicted to reflect their promoting activity and metabolism based on previous studies) (35–37,49,50) (Figure 3). The ratio of CYP1A1 and HO-1 mRNA levels to 18S

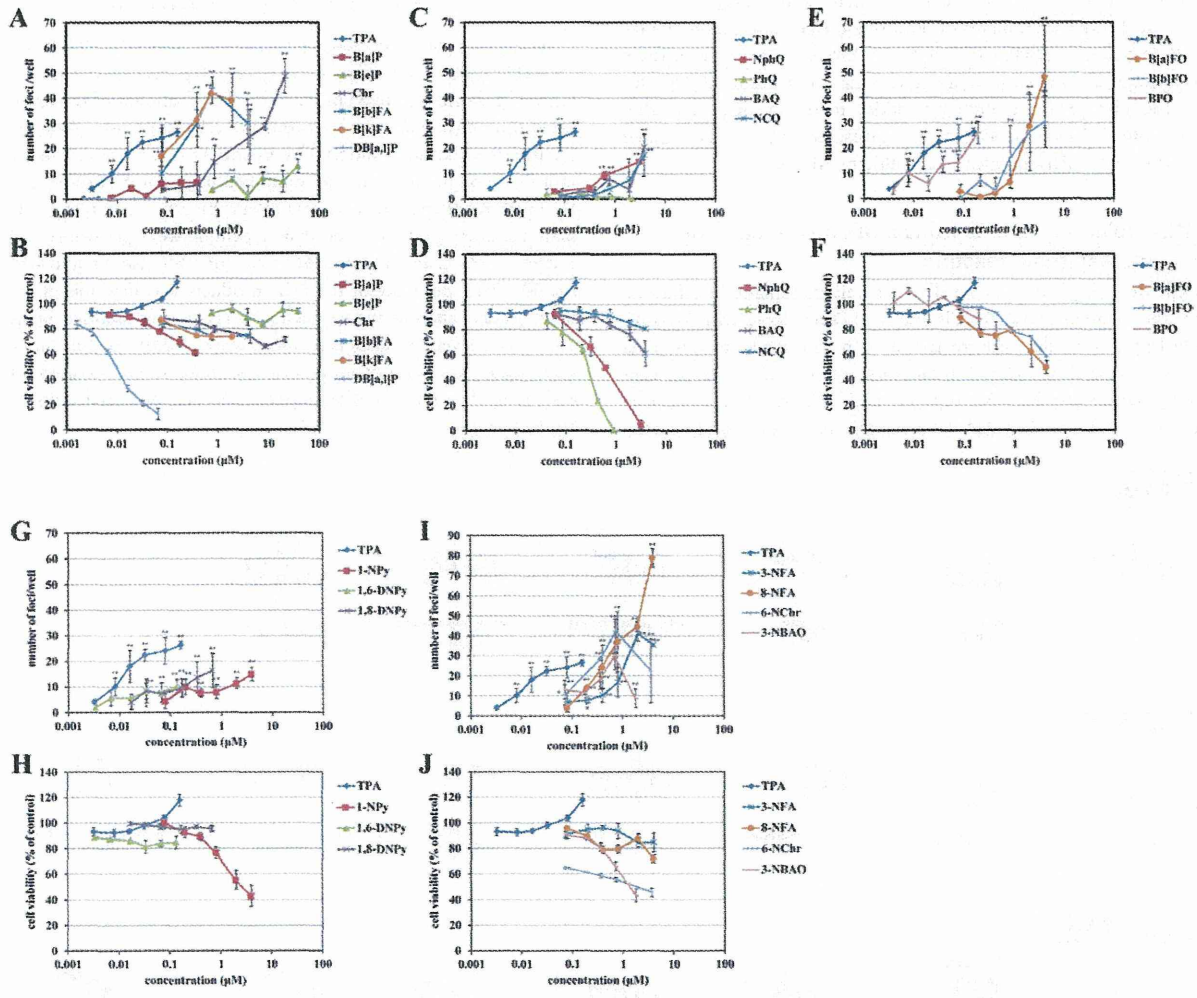

Figure 2. Tumour-promoting activity and cell viability of PACs. The tumour-promoting activities of (**A**) PAHs, (**C** and **E**) oxy-PAHs and (**G** and **I**) nitro-PAHs were measured using Bhas 42 cells. Cell viability for (**B**) PAHs, (**D** and **F**) oxy-PAHs and (**H** and **J**) nitro-PAHs in Bhas 42 cells was also examined. Double asterisks indicates highly significant differences from controls ($P < 0.01$) and single asterisk indicates significant differences from controls ($P < 0.05$), as determined by a Dunnett test.

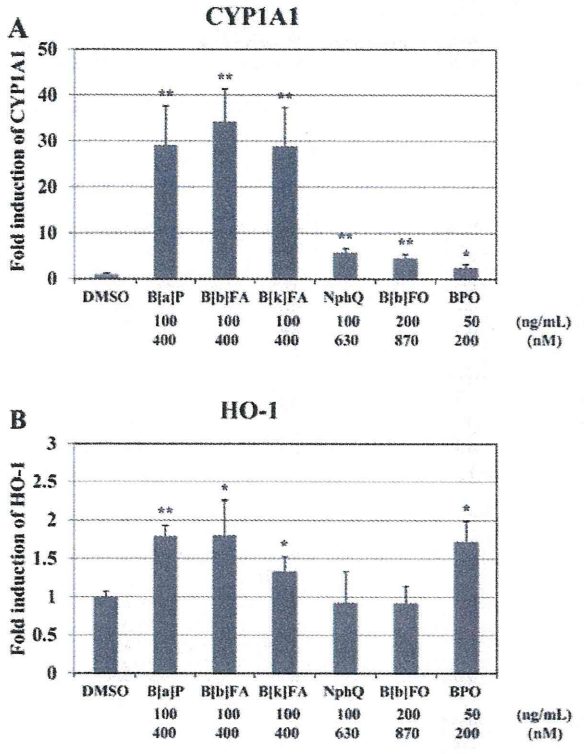

Figure 3. Induction of mRNA measured by RT-PCR using representative PAHs and oxy-PAHs. Bhas 42 cells were exposed to chemicals for 24h at concentrations at which significant tumour-promoting activities are known to be detected for these compounds (range 200 nM to 1 μM). (**A**) CYP1A1 mRNA and (**B**) HO-1 mRNA levels were measured. Double asterisks indicates highly significant differences from controls ($P < 0.01$) and single asterisk indicates significant differences from controls ($P < 0.05$), as determined by a Student's *t*-test.

rRNA of DMSO-treated control cells was 4.4×10^{-2} and 9.7×10^{-1}, respectively. Importantly, the concentration of compounds exposed to cells for mRNA detection was within the range 200 nM to 1 μM, in which significant tumour-promoting activity was detected using the Bhas 42 assay. CYP1A1 mRNA was induced by each of these compounds (Figure 3A). These three PAHs (B[*a*]P, B[*b*]FA and B[*k*]FA) induced CYP1A1 mRNA by 29-, 34- and 29-fold at 400 nM, respectively, in comparison with the DMSO-treated control. Of the oxy-PAHs, NphQ and B[*b*]FO exhibited moderate induction levels (6-fold at 630 nM and 5-fold at 870 nM, respectively), while at 200 nM, BPO showed a 2-fold higher induction of CYP1A1 mRNA than the control. HO-1 mRNA was significantly upregulated by treatment with three PAHs (B[*a*]P, B[*b*]FA and B[*k*]FA) and one oxy-PAH (BPO) (1.8-, 1.8-, 1.3- and 1.7-fold, respectively; Figure 3B). There was no significant change in induction levels of two oxy-PAHs (NphQ and B[*b*]FO) in comparison with the control. The present results (promoting activity) and previous toxic data, including AhR activity and CYP1A1 induction in hepatoma cells, are summarised in Table 1.

Discussion

Cancer is thought to be the result of several processes: initiation by exposure to mutagens, immortalisation, release of contact inhibition, acquisition of anchorage-independent growth, migration and metastasis ability. The release of contact inhibition is the most important step in the promotion process. In the present study, a transformation assay with Bhas 42 cells transfected with the *H*-ras gene from immortalised mouse foetus fibroblasts (BALB/3T3 cells) with contact inhibition abilities was used to assess the tumour-promotion process (29–31,51). Using this cell line, Asada *et al.* (29) detected tumour-promoting activity for B[*a*]A, Chr, B[*e*]P and 1-NPy. We also measured the tumour-promoting activity of the last three compounds and obtained comparable results, demonstrating that our experimental system is reproducible (Figure 2A and G). We evaluated the tumour-promoting activities of 16 other PACs for the first time (Figure 2).

The tumour-promoting activities of cells have been suggested to be mediated *via* the AhR-mediated pathway. Dietrich and Kaina (32) proposed that the release of cell-cell contact inhibition by 2,3,7,8-tetrachlorodibenzo-*p*-dioxin (TCDD) and PAHs was caused by cyclin A/cdk2-dependent cell cycle progression, mainly downstream of pRB with upregulation of p27 *via* AhR-mediated upregulation of cyclin A protein levels. They also suggested a potential role of AhR in the downregulation of E-cadherin (adherence junction), leading to epithelial-mesenchymal transition (EMT) and tumour progression (32). It was also suggested that the inhibition of gap junctional intercellular communication (GJIC) was in response to the downregulation of connexin levels *via* AhR activation in rat liver WB-F344 cells (34). In Bhas 42 cells, the decrease in GJIC and other contact inhibition systems may be caused by the AhR-mediated deregulation of genes related to intercellular adhesion following exposure to PACs. TCDD was also reported to disrupt the regulation of cell proliferation and apoptosis *via* several genes (p53, p27, cyclins, TGF-β, Ras and others) *via* AhR (32,33,52–54). Thus, AhR-mediated deregulation of cell growth and apoptosis may be the source of the tumour-promoting activity of Bhas 42 cells exposed to AhR-active PACs.

In the present study, we found for the first time high tumour-promotion activities of BPO, B[*k*]FA and B[*b*]FA and moderate activities of NphQ and B[*b*]FO (Figure 2A, C and E). A 24-h treatment with B[*b*]FA and B[*k*]FA prominently induced CYP1A1 mRNA, whereas NphQ and B[*b*]FO moderately induced the same gene in Bhas 42 cells (Figure 3A). These experimental findings support the results of AhR-mediated tumour-promoting activity.

In other cell lines, such as hepatoma cells, B[*k*]FA and B[*b*]FA have also been shown to have high AhR-mediated activities and CYP1A1 induction (Table 1) (35,40,41). AhR-mediated intermediate gene transcription activities have also been found for several oxy-PAHs, including NphQ and B[*b*]FO, using the CALUX assay and the CYP mRNA induction assay with HepG2 cells (39–41). It was predicted that many of the PACs inducing CYP mRNA in such hepatoma cells have tumour-promoting activities. Previous studies have exhibited a significant induction of CYPs by 6-NChr, dinitropyrenes, 3-NFA and 3-NBAO in human tissue-derived cells (21,37,38). In the present study, the tumour-promoting activities of these nitro-PAHs in Bhas 42 cells (Figure 2G) may have been mediated by AhR, particularly 6-NChr, which produced a high amount of CYPs.

The amount of CYP1A1 mRNA in response to a BPO treatment was only 2-fold greater than that of the DMSO-treated controls at the concentration at which significant tumour-promoting activity (increased number of foci) was confirmed (Figures 2E and 3A). However, in a previous study the induction of CYP1A1 mRNA in HepG2 cells was inhibited by 5 μM BPO (under half of the amount of the control) (41). Although differences in cell responses may be due to different amounts of metabolic enzymes and/or treated chemical concentrations, BPO seemed to be a weak inducer for CYP1A1 mRNA expression. Therefore, the powerful tumour-promoting activity of BPO could not be explained by only CYP1A1 mRNA induction but could be dependent on another pathway.